HHS Public Access

Author manuscript

Neuron. Author manuscript; available in PMC 2023 December 21.

Published in final edited form as:

Neuron. 2022 December 21; 110(24): 4125–4143.e6. doi:10.1016/j.neuron.2022.09.024.

Modulation of 5-HT release by dynorphin mediates social deficits during opioid withdrawal

Matthew B. Pomrenze[1], **Daniel F. Cardozo Pinto**[1], **Peter A. Neumann**[1], **Pierre Llorach**[2], **Jason M. Tucciarone**[1], **Wade Morishita**[1], **Neir Eshel**[1], **Boris D. Heifets**[2], **Robert C. Malenka**[1,3,*]

[1]Nancy Pritzker Laboratory, Department of Psychiatry and Behavioral Sciences, Stanford University, Stanford, CA 94305

[2]Department of Anesthesiology, Perioperative and Pain Medicine, Stanford University School of Medicine, Stanford, CA 94305

[3]Lead Contact

GRAPHICAL ABSTRACT

[*]Correspondence: malenka@stanford.edu (R.C.M.).

AUTHOR CONTRIBUTIONS

M.B.P. and R.C.M. conceived experiments, interpreted results and wrote the manuscript, which was edited by all authors. M.B.P. performed all behavioral assays, FISH assays, and fiber photometry recordings. D.F.C.P. performed anatomical assays and provided critical reagents. P.A.N. and J.M.T. assisted with histological analysis. P.L. assisted with behavioral assays. W.M. performed electrophysiological recordings. N.E. and B.D.H. provided technical expertise and assisted with data analysis.

DECLARATION OF INTERESTS

R.C.M. is on the scientific advisory boards of MapLight Therapeutics, Bright Minds, MindMed, Cyclerion, AZTherapies, and Aelis Farma. B.D.H. is on the scientific advisory boards of Osmind and Journey Clinical, and is a consultant for Clairvoyant Therapeutics and Vine Ventures. N.E. is a consultant for Boehringer Ingelheim.

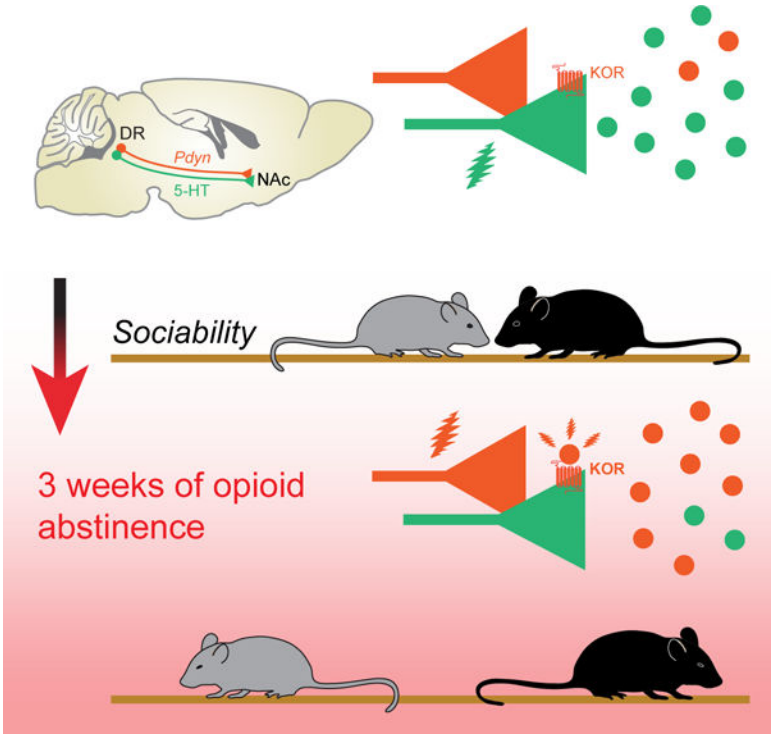

SUMMARY

Social isolation during opioid withdrawal is a major contributor to the current opioid addiction crisis. We find that sociability deficits during protracted opioid withdrawal in mice require activation of kappa opioid receptors (KORs) in the nucleus accumbens (NAc) medial shell. Blockade of release from dynorphin (*Pdyn*) expressing dorsal raphe neurons (DR^{Pdyn}), but not from NAc^{Pdyn} neurons, prevents these deficits in prosocial behaviors. Conversely, optogenetic activation of DR^{Pdyn} neurons reproduced NAc KOR-dependent decreases in sociability. Deletion of KORs from serotonin (5-HT) neurons, but not from NAc neurons or dopamine (DA) neurons, prevented sociability deficits during withdrawal. Finally, measurements with the genetically encoded $GRAB_{5\text{-}HT}$ sensor revealed that during withdrawal KORs block the NAc 5-HT release that normally occurs during social interactions. These results define a neuromodulatory mechanism that is engaged during protracted opioid withdrawal to induce maladaptive deficits in prosocial behaviors, which in humans contribute to relapse.

eTOC Blurb

Pomrenze et al. investigate how dynorphin and kappa opioid receptors promote social interaction deficits during protracted opioid withdrawal. They find that kappa receptors reduce social interaction during opioid abstinence by suppressing 5-HT release in the NAc, uncovering a neural mechanism that contributes to sociability deficits associated with opioid use disorder.

INTRODUCTION

Lethal overdoses from opioids have increased dramatically over the past decade, critically contributing to the “opioid crisis” in the United States (Florence et al., 2021; Keefe, 2021; Lembke, 2016). The COVID-19 pandemic has exacerbated the crisis by accelerating overdose deaths to unprecedented levels (>100,000 in the United States in 2020) (Kosten and Petrakis, 2021). Despite the societal costs of the opioid crisis and opioid use disorder (OUD) in general, prognosis remains poor because existing treatments are often inadequate in helping users maintain abstinence. The abstinent months and years following cessation of opioid use (i.e. during protracted opioid withdrawal) represent a period of high risk for relapse due to an array of associated symptoms including anhedonia, opioid cravings, and social avoidance (Epstein et al., 2009; Pantazis et al., 2021; Strang et al., 2020; Volkow and Blanco, 2021; Welsch et al., 2020). Periods of social isolation, as were precipitated by the COVID-19 pandemic, increase the risk of relapse and lethal overdose (Christie, 2021; Volkow, 2020). Indeed, the success of the community reinforcement approach, which encourages positive, adaptive social interactions and discourages social isolation (Abbott, 2009), indicates that unstable social conditions are significant determinants of opioid relapse and lethal overdose.

While initially driven by mu opioid receptors (MuORs) in reward circuits, repeated opioid consumption increasingly engages stress-related circuits that limit reward and drive maladaptive emotional states (Koob, 2008; Strang et al., 2020; Welsch et al., 2020). In contrast to MuORs, KORs and their endogenous ligand, the neuropeptide dynorphin, have well-established roles in stress, aversion, and negative affect (Bruchas et al., 2010; Crowley and Kash, 2015; Darcq and Kieffer, 2018; Lalanne et al., 2014; Lutz and Kieffer, 2013; Massaly et al., 2016; Tejeda et al., 2012; Van’t Veer and Carlezon, 2013; Wee and Koob, 2010). KOR antagonists reverse behavioral features of depression and aversion associated with stress and drug withdrawal in animals (Beardsley et al., 2005; Bruchas et al., 2011; Chartoff et al., 2012; Land et al., 2008; Land et al., 2009; Lemos et al., 2012; Mague et al., 2003; Massaly et al., 2019; McLaughlin et al., 2006; McLaughlin et al., 2003; Schindler et al., 2012; Schlosburg et al., 2013; Shirayama et al., 2004; Williams et al., 2018; Zachariou et al., 2006) and humans (Krystal et al., 2020), while KOR agonists are aversive and can produce social avoidance (Resendez et al., 2016; Resendez et al., 2012; Robles et al., 2014). Furthermore, during protracted opioid withdrawal, KORs have been implicated in the associated negative affective behaviors and social avoidance (Lalanne et al., 2017; Lutz et al., 2014) but the detailed mechanisms by which they function to influence sociability deficits during opioid withdrawal are poorly understood.

KORs are Gi-coupled receptors, which are widely expressed in the brain (DePaoli et al., 1994). Their presence in ventral tegmental area (VTA) DA neurons (Ford et al., 2006; Svingos et al., 2001) and in DR 5-HT neurons (Lemos et al., 2012) is of particular interest because release of these modulators in the NAc, a key component of classic mesolimbic reward circuitry, promotes prosocial behaviors (Dolen et al., 2013; Gunaydin et al., 2014; Heifets et al., 2019; Walsh et al., 2018) while infusions of KOR agonists into the NAc reduce extracellular levels of 5-HT and DA (Spanagel et al., 1992; Tao and Auerbach, 2002).

These findings suggest that KOR-mediated modifications in 5-HT and DA release dynamics may contribute to the social deficits observed during protracted opioid withdrawal.

To test this hypothesis, we implemented a protocol that generated robust sociability deficits in mice during protracted opioid withdrawal (Goeldner et al., 2011; Lutz et al., 2014) and used a variety of approaches including optogenetics, cell-type specific expression of transgenes, conditional deletion of KORs, and fiber photometry measurements of a genetically encoded 5-HT sensor, to examine the hypothesis that dynorphin action specifically in the NAc is a key mediator of withdrawal-associated social deficits. Our results support the conclusion that dynorphin release in the NAc from an unexpected and poorly characterized cell population in the DR is a critical mediator of the sociability deficits during protracted opioid withdrawal. This DR derived dynorphin binds to presynaptic KORs on DR 5-HT inputs resulting in a block of the increase in NAc 5-HT levels that normally accompanies prosocial interactions.

RESULTS

Social deficits during protracted morphine withdrawal

To model the sociability deficits that are frequently observed in humans during protracted opioid withdrawal (Strang et al., 2020; Volkow and Blanco, 2021), wild-type mice were administered escalating doses of morphine (MOR) (Zhu et al., 2016) and tested for prosocial behavior three weeks after cessation of MOR (Figure 1A). Consistent with previous reports (Bravo et al., 2020; Goeldner et al., 2011; Lalanne et al., 2017; Lutz et al., 2014), during this protracted opioid withdrawal, MOR-treated mice exhibited robust decreases in two well-established assays of prosocial behavior: the juvenile interaction test and the 3-chamber social preference test (Figures 1B–1E). To measure the acute responses to MOR, these same mice were placed into one side of a conditioned place preference (CPP) chamber following each MOR injection and tested for place preference 24 hr and 3 weeks later (Figure 1A). Consistent with the reinforcing nature of the MOR experience, a large preference for the MOR-paired side was observed at both time points (Figures 1F, S1A-S1C). Furthermore, MOR elicited a robust locomotor sensitization (Figures S1D and S1E), a behavioral adaptation that is associated with key features of the addicted state (Robinson and Berridge, 2003). To examine the specificity of the sociability deficits, we performed several additional behavioral assays: time spent interacting with a novel inanimate object, preference for an appetitive, palatable food pellet in the 3-chamber assay, and time spent in the center of an open field. Protracted MOR withdrawal produced no changes in any of these assays (Figures S1F-S1I).

The magnitude of the sociability deficits during protracted opioid withdrawal was highly correlated with the magnitude of the memory for the MOR experience. Specifically, the higher the MOR context preference, measured 3 weeks after cessation of MOR administration, the less time spent interacting with a juvenile (Figures 1G and 1H) and the lower the preference for the social chamber in the 3-chamber social preference assay (Figures 1I and 1J). Even numbers of female and male subjects were included in each group and sub-analyses revealed no sex differences (Figures S1J-S1Q). Correlations were also preserved when analyzed for females and males separately (Figures S1R-S1U). These

results suggest that social avoidance behavior during protracted opioid withdrawal strongly correlates with the “memory” of the drug experience and therefore may contribute to an individual’s propensity to relapse.

NAc medial shell KORs are necessary for sociability deficits during withdrawal

KOR activation contributes to stress-induced cocaine seeking and appears to be necessary for some of the social deficits during protracted opioid withdrawal (Lalanne et al., 2017; Land et al., 2008; Land et al., 2009; Lutz et al., 2014; Redila and Chavkin, 2008; Schindler et al., 2012). However, it is unknown which specific brain regions express the KORs that are required for the social behavior changes caused by chronic opioid administration. Given that the NAc contains dynorphin-expressing neurons and receives inputs from DA and 5-HT neurons that play a role in prosocial behavior (Dai et al., 2022; Gunaydin et al., 2014; Heifets et al., 2019; Walsh et al., 2018), we tested if KORs specifically in the NAc medial shell are necessary for social deficits during protracted opioid withdrawal. Guide cannula were implanted bilaterally in the NAc medial shell and following baseline sociability testing, mice were subjected to the chronic MOR administration regimen (Figure 1K). Three weeks after cessation of MOR administration, sociability assays were performed and then mice were randomly split into groups receiving either a microinjection of saline or the long-lasting KOR antagonist norbinaltorphimine (norBNI; 2.5 μg/hemisphere). Sociability testing 24 hr later revealed that the saline injected subjects still exhibited robust deficits in both social assays while these deficits were reversed by the norBNI treatment (Figures 1L–1O).

We next addressed whether a KOR antagonist that is being evaluated in humans, Aticaprant (JNJ-67953964, previously CERC-501 and LY2456302; Krystal et al., 2020), was also effective in ameliorating social deficits during protracted withdrawal. We systemically administered Aticaprant (3 mg/kg, ip) or vehicle in a counterbalanced crossover design before both social assays that were performed 48 hours apart during withdrawal as well as before a CPP posttest (Figure S2A). Consistent with the effects of infusing norBNI into the NAc, Aticaprant reversed sociability deficits during withdrawal and also reduced MOR chamber preference (Figures S2B-S2F).

A potential source for the dynorphin that activates KORs in the NAc during opioid withdrawal are D1 receptor-expressing medium spiny neurons (MSNs), a major proportion of which express dynorphin (NAc^{Pdyn} neurons) (Al-Hasani et al., 2015). To test if dynorphin release from NAc^{Pdyn} neurons is necessary for the sociability deficits during protracted opioid withdrawal, we injected adeno-associated virus (AAV) carrying a Cre-dependent tetanus toxin (AAV-DIO-TeTx-p2A-eGFP) or eGFP alone as a control (AAV-DIO-eGFP) into the NAc medial shell of *Pdyn*-Cre mice (Figures 2A and 2B). Tetanus toxin (TeTx) “silences” neurons by preventing SNARE-dependent release of transmitters due to cleavage of the critical SNARE protein VAMP/synaptobrevin (Kim et al., 2009). Surprisingly, mice expressing TeTx in NAc^{Pdyn} neurons showed normal baseline social behaviors (Figures S2H and S2I) and still exhibited robust sociability deficits during protracted withdrawal, which were similar to those in mice expressing eGFP in NAc^{Pdyn} neurons (Figures 2C–2F). The TeTx animals also exhibited normal CPP both 24 hr and 3 weeks after MOR

administration (Figures 2G, S2J and S2K). However, MOR-induced locomotor sensitization was significantly reduced (Figures S2L and S2M), indicating that the TeTx manipulation was effective in these same animals. Consistent with the results from the initial cohort of animals, there was an inverse correlation between the magnitude of the sociability deficits and the magnitude of the preference for the chamber in which MOR was experienced (Figures S2N and S2O). To further examine if TeTx expression adequately reduced transmitter release from NAc MSNs we recorded stimulation evoked and spontaneous inhibitory postsynaptic currents (IPSCs) from uninfected and infected NAc MSNs in slices prepared from animals that had received unilateral injections of AAV-TeTx-eGFP in the NAc medial shell (Figure S2P). Consistent with the established effects of TeTx, evoked and spontaneous IPSCs were almost entirely absent in NAc MSNs expressing TeTx and recorded in the NAc medial shell compared to recordings in uninfected NAc MSNs from the opposite hemisphere (Figures S2P-S2U).

DR^{Pdyn} neurons regulate sociability through KOR activation in NAc

Where might the dynorphin that is presumably released in the NAc during protracted opioid withdrawal derive? Examination of the Allen Mouse Brain Atlas revealed that *Pdyn* is expressed in many brain regions that send projections to the NAc including the DR (Lein et al., 2007). Because 5-HT release in the NAc from DR neurons is critical for prosocial behavior (Heifets et al., 2019; Walsh et al., 2018), we were interested in the possibility that there may be a population of NAc-projecting dynorphin neurons in the DR (DR^{Pdyn} neurons). Consistent with this prediction, injection of AAV expressing Cre-dependent eYFP into the DR of *Pdyn*-Cre mice (Figure 2H) revealed a robust projection to the NAc medial shell, particularly in the dorsomedial region and more diffusely in the ventromedial shell (Figure 2I). Injection of AAV expressing Cre-dependent mGFP-p2A-synaptophysin-mRuby into the DR confirmed the presence of many putative release sites in DR^{Pdyn} axons in the NAc medial shell (Figures S3A and S3B).

To test whether transmitter release from DR^{Pdyn} neurons is necessary for the sociability deficits during protracted opioid withdrawal, *Pdyn*-Cre mice were injected with AAV-DIO-TeTx-p2A-eGFP into the DR and run through the same MOR administration and withdrawal procedures (Figure 2J). In marked contrast to expression of TeTx in NAc^{Pdyn} neurons, expressing TeTx in DR^{Pdyn} neurons prevented the decrease in prosocial behaviors that routinely occurs during protracted withdrawal (Figures 2K–2N). These same TeTx mice still exhibited a strong initial preference for the MOR-paired chamber and locomotor sensitization (Figures S3D-S3G). However, they showed a reduced preference for the MOR-paired context during the withdrawal CPP test (Figure 2O). Correlation analyses revealed a significant relationship between MOR CPP and sociability deficits in eGFP mice but this correlation was disrupted in TeTx mice (Figures S3H and S3I). Together these results suggest that DR^{Pdyn} neurons are a critical source for the dynorphin in the NAc that is required for the sociability deficits during protracted opioid withdrawal and also contribute to the prolonged memory of the MOR experience.

In addition to preventing sociability deficits during protracted opioid withdrawal, TeTx expression in DR^{Pdyn} increased baseline sociability in the juvenile intruder assay with a

trend toward an increase in the 3-chamber task (Figures S3J and S3K), suggesting that dynorphin release from this cell population may normally reduce or limit prosocial behavior. To test this prediction, we injected AAV expressing Cre-dependent ChR2 (AAV-DIO-ChR2) or eYFP (AAV-DIO-eYFP) as a control into the DR of *Pdyn*-Cre mice and implanted an optical fiber in the same location (Figure 3A). Optogenetic activation of DR^{Pdyn} neurons robustly reduced social interaction and social preference (Figures 3B–3E), but produced no reinforcement or aversion on its own in a real time place preference test (Figure 3F). Importantly, the same stimulation in the same mice did not affect investigation of a novel object, preference for a chamber containing a high-fat food pellet, or time spent in the center and locomotor activity in the open field (Figures S4A-S4E). We next evaluated the effect of stimulating DR^{Pdyn} inputs specifically in the NAc medial shell by placing fibers above this NAc subregion (Figure 3G). This manipulation mimicked the effects of DR^{Pdyn} neuron cell body stimulation in that it again reduced prosocial behavior in both assays (Figures 3H–3K) and also did not produce a reinforcement or aversion in a real time place preference assay (Figure S4G). Furthermore, stimulation of this pathway did not affect center time or locomotor activity in the open field (Figures S4H and S4I).

To examine if dynorphin release in NAc medial shell from DR^{Pdyn} neurons and the consequent activation of NAc KORs are required for the behavioral effects of activating this cell population, we combined optogenetic activation of DR^{Pdyn} cell bodies with microinfusion of norBNI or saline into the NAc medial shell (Figure 3L). Since norBNI can inhibit KOR signaling *in vivo* for several weeks (Bruchas et al., 2007), we implemented a procedure that enabled within-subject comparisons (Figure 3L). All mice initially received NAc medial shell infusions with saline, which 24 hours later did not influence the reductions in prosocial behaviors elicited by cell body optogenetic activation of DR^{Pdyn} neurons (Figures 3M–3Q). A week later, half the mice again received saline infusions while the other half received norBNI, a manipulation which blocked the sociability deficits generated by optogenetic activation of DR^{Pdyn} neurons (Figures 3M–3Q). Importantly, in the saline treated mice, this same manipulation again caused robust sociability deficits (Figures 3M–3Q). These results demonstrate that DR^{Pdyn} cell stimulation reduces prosocial behaviors due to KOR signaling in the NAc medial shell.

$DR^{5\text{-}HT}$ and DR^{Pdyn} neurons send parallel projections to NAc medial shell

The DR contains multiple different cell types with a majority of these being 5-HTergic as evidenced by their expression of tryptophan hydroxylase 2 (TPH2) (Zhang et al., 2004). The DR also has a small population of DA neurons, which have been implicated in social behavior, arousal, pain, and reward memory (Cho et al., 2017; Lin et al., 2020; Matthews et al., 2016; Yu et al., 2021). Given the importance of 5-HT and DA in social behaviors, an important question is whether DR^{Pdyn} neurons are capable of co-releasing 5-HT or DA. To address this issue, we crossed *Pdyn*-Cre mice with Ai14 reporter mice so that *Pdyn* cells expressed tdTomato (tdTom) and then stained DR tissue from these mice for TPH2 and tyrosine hydroxylase (TH) (Figure 4A). While <1% of DR^{Pdyn} neurons co-localized with TH (data not shown), consistent with a previous report (Lemos et al., 2012) ~42% of DR^{Pdyn} neurons were 5-HTergic as defined by their co-expression of TPH2 (Figure 4B). The complimentary analysis revealed that ~30% of 5-HTergic neurons (i.e. TPH2+ neurons)

were *Pdyn*+ (i.e. tdTomato+) (Figure 4C). Sub-analyses revealed no sex differences in these expression profiles (Figures S5A-S5D). The distribution of DR^{Pdyn} neurons was similar across the AP axis of the DR, while *Pdyn*+/5-HT+ cells were clustered medially in the mid and caudal aspects of the DR (Figures 4D and 4E). *Pdyn* neurons not expressing TPH2 were clustered laterally in the anterior DR, with a gradient of cells spreading into the neighboring vlPAG. The caudal DR, on the other hand, contained a large cluster of intermingled 5-HT+ and 5-HT- *Pdyn* neurons. Overall, this *Pdyn* expression pattern in 5-HT neurons is consistent with single-cell RNA sequencing studies reporting this gene in several major 5-HT cell clusters (Huang et al., 2019; Okaty et al., 2020; Ren et al., 2019).

To map the projection fields of these DR populations, we crossed *Pdyn*-Cre mice to *Sert*-Flp mice, which express Flp in 5-HT neurons (Ren et al., 2019). Injection of a cocktail of AAV-DIO-mCherry and AAV-fDIO-eYFP into the DR of *Pdyn*-Cre:*Sert*-Flp mice (Figure 4F) revealed *Sert*+ and *Pdyn*+ projections to the ventral tegmental area (VTA), basolateral amygdala (BLA), bed nucleus of the stria terminalis (BNST), NAc, and anterior prelimbic cortex (Figures S5E-S5J), consistent with previous work (Cardozo Pinto et al., 2019). Axonal projection patterns of the two major cell-types were generally similar with *Pdyn* axons more medially biased and restricted. In the NAc, *Sert*+ inputs were diffuse across the medial shell, lateral shell, and core while *Pdyn* inputs were heavily concentrated in the medial shell (Figure 4G). To further examine this anatomical specificity, *Pdyn*-Cre:*Sert*-Flp mice were injected in the DR with either AAV-CreON-FlpOFF-eYFP to label *Pdyn* only cells, AAV-CreOFF-FlpON-eYFP to label *Sert* only cells, or AAV-CreON-FlpON-eYFP to label neurons that are both *Pdyn*+ and *Sert*+ (Figures 4H–4P). Inputs from *Pdyn* only DR neurons in the NAc were found innervating the medial border of the medial shell from the dorsal cone to the ventral region (Figure 4I), whereas inputs from *Sert* only DR neurons encompassed the entire NAc shell and encroached into the core (Figure 4L). *Pdyn+/Sert+* DR inputs were found throughout the medial shell, with the densest axon field in the dorsal region (Figure 4O). Viral infection of cell bodies in the DR matched the predicted distribution across the AP axis from our co-localization data with *Pdyn*-Cre:Ai14 mice (Figures 4J, 4M, and 4P). These tracing data demonstrate three parallel projections to the NAc emanating from 3 subtypes of DR neurons with *Pdyn* inputs preferentially innervating the dorsomedial shell, compared to broader 5-HT inputs innervating the entire shell and core.

KORs in 5-HT neurons are necessary for sociability deficits during opioid withdrawal

The finding that norBNI infusion into the NAc medial shell reverses the sociability deficits during protracted opioid withdrawal indicates that cellular elements within the NAc must express the requisite KORs but does not distinguish between KORs on local NAc neurons/glia versus KORs on presynaptic inputs. To examine whether KORs on intrinsic NAc neurons are necessary for the sociability deficits, we selectively ablated local NAc KORs by injecting AAV-Cre-eGFP into the NAc of floxed KOR ($Oprk1^{fl/fl}$) mice and compared their behaviors during protracted opioid withdrawal with $Oprk1^{fl/fl}$ mice that were injected with AAV-ΔCre-eGFP (Figure 5A). Mice expressing the active Cre and therefore lacking KORs in the NAc medial shell exhibited sociability deficits that were essentially identical to those exhibited by $Oprk1^{fl/fl}$ mice injected with the control virus (Figures 5B–5E). These same

animals also exhibited normal locomotor sensitization and MOR reward learning in the CPP procedure (Figures S6A-S6E), which persisted 3 weeks into withdrawal (Figure 5F), as well as an inverse correlation between MOR CPP and sociability (Figures S6F and S6G).

5-HT and DA inputs to the NAc play key roles in social behaviors (Gunaydin et al., 2014; Walsh et al., 2018) and activation of KORs in the NAc reduces extracellular 5-HT (Tao and Auerbach, 2002) and DA (Spanagel et al., 1992). Moreover, KOR activation suppresses 5-HT release from synaptosome preparations extracted from the NAc (Schindler et al., 2012). We therefore hypothesized that KORs on 5-HT or DA inputs to the NAc are critical for the sociability deficits during protracted opioid withdrawal. While KOR expression in DA neurons is well established (Tejeda and Bonci, 2019), KOR expression in 5-HT neurons is still unclear. To determine if NAc-projecting DR 5-HT neurons express KORs, we injected fluorescent cholera toxin B (CTB-647) into the NAc medial shell of wild-type mice and harvested tissue for fluorescence *in situ* hybridization (FISH) (Figure 5G). CTB-647 preferentially labeled a population of neurons that localized to the dorsomedial aspect of the caudal DR (cDR; Figures 5H–5J). Few retro-labeled cells were found in the anterior or central DR (Figures 5I). FISH revealed that >90% of these NAc-projecting neurons in the cDR expressed *Sert* (*Slc6a4*), identifying them as 5-HTergic (Figure 5J). *Oprk1*, the mRNA encoding KORs, was detected in cells throughout the DR but many of these were *Sert*- and not labelled by CTB-647 (Figures 5I and 5J). The vast majority of the NAc-projecting *Sert*+ neurons that were also *Oprk1+* were in the cDR (Figures 5H and 5J). Reanalysis of a recent single-cell RNAseq dataset from DR cells (Huang et al., 2019) revealed a similar result in that *Oprk1* was expressed in all cell-types in the DR with the highest *Oprk1* expression in 5-HT neurons found in the 5-HT neuron cluster localized to the caudal DR (data not shown). Consistent with an independent DR single-cell RNAseq paper (Ren et al., 2019), *Oprk1* expression was minimal in all other 5-HT neuron subtypes, which project to other brain areas. These anatomical analyses identify a special NAc-projecting subpopulation of 5-HT neurons that express KORs and therefore may be influenced by dynorphin.

To directly test whether KORs expressed specifically in 5-HT neurons are necessary for the sociability deficits during protracted opioid withdrawal, we crossed *Oprk1*$^{fl/fl}$ mice with *Sert*-Cre mice (Figure 5K). Homozygous 5-HT KOR knockout mice generated by this cross exhibited basal levels of social interaction and social preference that were similar to wild-type littermates (Figures 5L and 5N). However, the decreases in these measures that normally occur during protracted opioid withdrawal were absent (Figures 5L–5O). These same KOR knockout mice also exhibited a blunted preference for the MOR-paired chamber during withdrawal (Figure 5P) although locomotor sensitization and the initial MOR CPP were normal (Figures S6H-S6K). Furthermore, while the wild-type control mice exhibited the expected inverse correlation between the magnitude of MOR CPP and sociability, the KOR knockout mice did not (Figures S6L and S6M). FISH confirmed genetic deletion of *Oprk1* from 5-HT neurons (Figures S6N-S6P).

To test whether KORs in DA neurons (Figures 5Q and 5R) are also required for the withdrawal sociability deficits, we crossed *Oprk1*$^{fl/fl}$ mice with *Dat*-Cre mice (Figure 5S). These homozygous DA KOR knockout mice did not differ from littermate controls in that they exhibited comparable sociability deficits during withdrawal (Figures 5T–5W), normal

locomotor sensitization (Figures S6Q and S6R) as well as normal place preference initially (Figures S6S and S6T) and during withdrawal (Figure 5X). Furthermore, there was an inverse correlation between the magnitude of MOR CPP and sociability during withdrawal (Figures S6U and S6V). *Oprk1* knockout was verified with FISH (Figures S6W-S6Y). Together, these results identify a requisite, selective role for KORs in 5-HT neurons in the social avoidance phenotype associated with protracted opioid withdrawal.

KORs suppress 5-HT release in the NAc during protracted opioid withdrawal

Given the importance of 5-HT release in the NAc for prosocial behavior (Heifets et al., 2019; Walsh et al., 2018), all of the results presented thus far are consistent with the hypothesis that prolonged opioid withdrawal leads to increased dynorphin release in the NAc, which in turn reduces 5-HT release during social interactions due to activation of KORs on $DR^{5\text{-}HT}$ inputs. To further examine this hypothesis, we directly measured 5-HT release dynamics by performing fiber photometry in wild-type mice expressing the genetically encoded fluorescent 5-HT sensor $GRAB_{5\text{-}HT}$ (Wan et al., 2021) in the NAc medial shell. To test and presumably confirm the utility of this approach, we initially performed pharmacological manipulations (Figure 6A). Administration of MDMA (3,4-Methylenedioxymeth-amphetamine, 7.5 mg/kg, ip), which is known to cause large increase in 5-HT levels (Green et al., 2003), generated a robust increase in NAc medial shell $GRAB_{5\text{-}HT}$ fluorescence (Figures S7A-S7C). In contrast, the KOR agonist U-50488 (5 mg/kg, ip) decreased $GRAB_{5\text{-}HT}$ fluorescence (Figures 6B and 6C), concomitant with a reduction in transient event frequency and amplitude, all of which were blocked by pretreatment with norBNI (10 mg/kg, ip) (Figures 6B–6E).

We next recorded NAc medial shell $GRAB_{5\text{-}HT}$ fluorescence during social interactions using the juvenile intruder assay (Figure 6F). During baseline measurements, transient increases in $GRAB_{5\text{-}HT}$ fluorescence occurred during initial social contact in two independent groups of mice (Figure 6G), a result consistent with the increases in $DR^{5\text{-}HT}$ neuron activity that occur during similar social interactions (Walsh et al., 2018). These same mice then received our standard saline or escalating MOR treatments and three weeks into protracted withdrawal were imaged again during an identical juvenile interaction test. MOR treated mice exhibited a decrease in $GRAB_{5\text{-}HT}$ fluorescence during their social interactions while saline treated mice exhibited increases that were similar to those observed during baseline measurements (Figures 6H–6J). Subsequent administration of norBNI in the MOR treated mice resulted in recovery of $GRAB_{5\text{-}HT}$ fluorescence to normal levels during social contact (Figures 6K–6O) and, as expected, an increase in the total duration of the social interactions (Figure S7D). Because DA levels in the NAc also increase during social interactions (Dai et al., 2022; Wang et al., 2021), we repeated these same experiments in mice in which $GRAB_{DA}$ (Sun et al., 2020) was expressed in NAc medial shell (Figure S7E). Similar to $GRAB_{5\text{-}HT}$ fluorescence, NAc medial shell $GRAB_{DA}$ fluorescence increased during baseline social interactions (Figure S7F) but this increase was not significantly reduced during social interactions three weeks into protracted opioid withdrawal (Figures S7G-S7I).

To further test if KOR signaling specifically in 5-HT neurons mediates the reduction in 5-HT release that occurs during social interactions in mice experiencing protracted

withdrawal, we expressed $GRAB_{5\text{-}HT}$ in the NAc medial shell of homozygous 5-HT KOR knockout mice (Figure 7A). Knockout mice and controls displayed the expected increase in NAc $GRAB_{5\text{-}HT}$ fluorescence during baseline social contact (Figure 7B). However, during protracted opioid withdrawal, the knockout mice continued to exhibit a clear increase in $GRAB_{5\text{-}HT}$ fluorescence during social contact while, consistent with our previous results, the control mice did not (Figures 7C-7E). Furthermore, as expected, the sociability deficits during withdrawal were present in the control mice but absent in the knockout mice (Figure S7J).

Because the KOR-mediated reduction of 5-HT release during social interactions is happening within the NAc, changes in the physiology of $DR^{5\text{-}HT}$ neurons themselves during withdrawal are not required to account for any of our results, but nevertheless could importantly contribute (Walsh et al., 2018), especially given that KOR activation can suppress $DR^{5\text{-}HT}$ neuron excitability (Lemos et al., 2012). To address this topic, we injected AAV-DIO-GCaMP6m into the DR of *Sert*-Cre mice and recorded $DR^{5\text{-}HT}$ neuron activity during baseline social interactions and when the mice were experiencing protracted opioid withdrawal (Figure 7F). During prolonged opioid withdrawal, in contrast to the dramatic decreases in NAc $GRAB_{5\text{-}HT}$ fluorescence during social interactions, there was no detectable change in the increase in $DR^{5\text{-}HT}$ neuron GCaMP6m fluorescence (Figures 7G-7J) even though there was the expected decrease in social interaction times (Figure S7K). Thus, sociability deficits during protracted opioid withdrawal and in an autism model (Walsh et al., 2018) both appear due to a decrease in NAc 5-HT release during prosocial interactions but these decreases are mediated via different mechanisms.

DISCUSSION

We have presented a series of results, all of which are consistent with the hypothesis that protracted opioid withdrawal generates an increase in NAc medial shell dynorphin, which derives specifically from DR^{Pdyn} neurons, resulting in activation of KORs on inputs from $DR^{5\text{-}HT}$ neurons. Activation of these presynaptic KORs in turn decreases NAc medial shell 5-HT levels during social interaction, leading to reduced sociability. This hypothesis is supported by prior work showing that: (1) optogenetic inhibition of $DR^{5\text{-}HT}$ inputs in the NAc reduces prosocial behaviors (Walsh et al., 2018); (2) dynorphin infusion into the NAc reduces 5-HT levels (Tao and Auerbach, 2002); and (3) systemic administration of a KOR antagonist reduces social deficits during opioid withdrawal in mice (Lalanne et al., 2017; Lutz et al., 2014).

There is an extensive literature on the contributions of dynorphin and KORs to stress-induced behavioral adaptations and other forms of aversive or appetitive motivated behaviors with more recent studies suggesting that the behavioral consequences of dynorphin signaling in the NAc are quite complex (Castro and Bruchas, 2019). For example, optogenetic stimulation of NAc^{Pdyn} neurons caused either a real time place preference or real time avoidance depending on their specific location within the NAc (Al-Hasani et al., 2015). Similarly, infusion of a KOR agonist into the NAc increased or decreased hedonic “liking” responses to sucrose depending on the exact infusion location (Castro and Berridge, 2014). Our finding that dynorphin release from DR^{Pdyn}, but not NAc^{Pdyn}, neurons is required for

the sociability deficits during protracted withdrawal but does not elicit a place preference or place avoidance suggests that the source of the dynorphin released in the NAc is also a critical factor in determining the behavioral consequences of NAc dynorphin signaling. Apparently, the dynorphin released from DR^{Pdyn} neurons has preferential access to the KORs on the 5-HT inputs driving increases in prosocial behaviors. This may be due to the ~30% of $DR^{5\text{-}HT}$ neurons that also express *Pdyn* and presumably release dynorphin and also because KORs appear to be expressed on a subpopulation of $DR^{5\text{-}HT}$ neurons with relatively restricted projections to subregions of the NAc.

One limitation of our study is that the exact mechanism of enhanced KOR activity in NAc 5-HT inputs during protracted opioid withdrawal is unknown. norBNI acts as an inverse agonist that triggers a non-competitive persistent inhibition of KOR signaling via initiation of the c-Jun N-terminal Kinase pathway (Bruchas et al., 2007; Melief et al., 2010). This unique property bypasses traditional competitive antagonism by triggering a competing biochemical cascade as opposed to blocking agonist binding. This distinction is important since acute stress can trigger constitutive activity of KORs on inhibitory inputs to VTA DA neurons that lasts for weeks and promotes cocaine reinstatement (Graziane et al., 2013; Polter et al., 2017; Polter et al., 2014). Since norBNI reduces the signaling capacity of KORs regardless of constitutive activity or dynorphin binding, it remains unclear which mechanism enhances KOR activity in the NAc during protracted withdrawal. However, the prevention of sociability deficits by the short-acting competitive antagonist Aticaprant suggests that increases in NAc dynorphin levels during prolonged withdrawal likely mediate the effects we have observed.

Unlike classic neurotransmitters and neuromodulators such as glutamate, GABA, DA and 5-HT, neuropeptides such as dynorphin generally do not undergo active uptake but rather are degraded extracellularly by peptidases (van den Pol, 2012). This facilitates non-classic forms of non-synaptic signaling and allows neuropeptides to often act at long distances from their release sites (Castro and Bruchas, 2019; van den Pol, 2012). Although we have provided evidence that dynorphin release from DR^{Pdyn}, but not NAc^{Pdyn}, neurons, is critical for the sociability deficits during protracted opioid withdrawal, we cannot rule out that additional sources of dynorphin from cortical inputs or *Pdyn* neurons in the NAc ventral shell might also contribute to maladaptive behaviors during opioid withdrawal (Al-Hasani et al., 2015; Massaly et al., 2019). Furthermore, during the course of this project, two papers appeared reporting DR^{Pdyn} neurons projecting to the VTA where they regulate DA neuron activity to promote fear generalization (Fellinger et al., 2021) and enhance cocaine reward after stress (Abraham et al., 2022). Whether these DR^{Pdyn} neuron projections to the VTA influence social behavior during opioid withdrawal via modulation of DA neurons is unknown, but the lack of changes in $GRAB_{DA}$ measurements during withdrawal suggest that they do not. Clearly, for a more comprehensive mechanistic understanding of why dynorphin's actions in the NAc, and perhaps other structures such as the VTA, appear to depend on the source from which it is released, more detailed knowledge about its release sites, release mechanisms and diffusion will be necessary combined with greater understanding of the location and functions of the KORs upon which it acts. Recent advances in fluorescent neuropeptide sensor technologies could shed light on these complex mechanisms (Abraham et al., 2021).

Previous work suggests that release of 5-HT in the NAc from $DR^{5\text{-}HT}$ neurons is enhanced by oxytocin resulting in the promotion of social reward (Dolen et al., 2013). Thus, by modulating NAc 5-HT levels in opposite directions during social interactions, two different neuropeptides, oxytocin and dynorphin, both influence social behaviors in opposite directions. The negative feedback on 5-HT release by dynorphin may help regulate the degree and duration of social approach behavior as well as other behaviors influenced by NAc 5-HT release. Both oxytocin and dynorphin also influence NAc DA signaling in opposite directions: oxytocin by exciting VTA DA neurons (Hung et al., 2017) and dynorphin by inhibiting DA release via presynaptic KORs (Pirino et al., 2020; Spanagel et al., 1992) as well as by inhibiting VTA DA neuron activity (Ehrich et al., 2015; Ford et al., 2006). However, we find that changes in NAc DA release during social interactions did not contribute to the sociability deficits during protracted opioid withdrawal. Furthermore, unlike DA release in the NAc, 5-HT release in the NAc does not function as a reinforcer that drives instrumental conditioning (Walsh et al., 2018). These results are all consistent with the proposition that unlike NAc DA release, NAc 5-HT release plays a relatively specific role in prosocial behaviors. Consistent with this proposal, we found that optogenetic activation of DR^{Pdyn} neurons had no effect on subjects' interactions with an inanimate object or non-social appetitive objects such as high caloric food (Figure S4; Walsh et al. 2018).

While we have observed robust changes in social behavior and 5-HT dynamics after passive administration of high doses of MOR, it is possible that self-administration of MOR or other opioids may elicit different neuroadaptations and behavioral effects. We predict that similar adaptations will occur since KOR signaling in the NAc is critical for the escalated motivation to self-administer heroin in long-access paradigms, which are associated with increased dynorphin content in the NAc medial shell (Schlosburg et al., 2013). Nevertheless, the route of administration as well as amount of drug consumed are likely to be critical factors for the development of OUD. Thus, in future work it will be important to determine whether prolonged abstinence from opioid self-administration produces similar deficits in sociability and 5-HT release in the NAc, and if so, whether these maladaptive changes are key drivers of relapse.

Alterations in 5-HT signaling in the DR and NAc during withdrawal from chronic opioid consumption in rodents have been observed previously (Goeldner et al., 2011; Harris and Aston-Jones, 2001; Lutz et al., 2011; Tao et al., 1998). Similarly, dynorphin levels increase in the NAc and amygdala in various rodent models of addiction (Carlezon et al., 1998; Zachariou et al., 2006; Zan et al., 2021). While medications such as the SSRI fluoxetine and 5-HT receptor agonists such as lorcaserin have efficacy in reducing withdrawal symptoms in rodents, the usefulness of lorcaserin and standard antidepressants such as SSRIs in treating the emotional deficits associated with addiction has been limited (https://clinicaltrials.gov/ct2/show/study/NCT03007394; Nunes and Levin, 2006). Buprenorphine, currently considered the treatment of choice for OUD, was initially pursued because it activates MuORs and thereby may function as an opioid substitute, similar to methadone (Bart, 2012; Blanco and Volkow, 2019). However, it also functions as a KOR antagonist, an action that may contribute to its efficacy in treating OUD as evidenced by the efficacy of systemic norBNI administration to reverse social impairments in mice during withdrawal from chronic heroin exposure (Lalanne et al., 2017). Our results describe an unexpected,

highly specific mechanism for this therapeutic action of KOR antagonism in ameliorating the deficient prosocial behavior and social isolation during prolonged abstinence, which in humans with OUD importantly contributes to relapse (Christie, 2021; Heilig et al., 2016; Humphreys et al., 2022; Strang et al., 2020) and has been exacerbated by COVID-19 (Marsden et al., 2020). They suggest that further detailed understanding of the actions of NAc dynorphin release from DR^{Pdyn} neurons as well as more thorough investigation of the role of heterogeneous DR inputs to the NAc in motivated behaviors (Castro et al., 2021) may provide important clues to additional novel therapeutic interventions. For example, in addition to targeting KORs, our results suggest that interventions that robustly enhance 5-HT signaling in the NAc in a manner that promotes sociability (Heifets and Malenka, 2021; Walsh et al., 2021) might help humans with OUD become more willing to accept social support and seek treatment.

STAR*METHODS

Detailed methods are provided in the online version of this paper.

Lead contact

Further information and requests for resources and reagents should be directed to and will be fulfilled by the lead contact, Dr. Robert C. Malenka (malenka@stanford.edu).

Materials availability

This study did not generate new unique reagents.

Data and code availability

The datasets generated and/or analyzed in the current study are available from the lead contact upon reasonable request. This paper does not report original code. Any additional information required to reanalyze the data reported in this paper is available from the lead contact upon request.

EXPERIMENTAL MODEL AND SUBJECT DETAILS

Subjects

Female and male C57BL/6J (Jackson Laboratory; stock #00664), heterozygous *Pdyn*$^{tm1.1(cre)Mjkr}$/LowlJ (*Pdyn*-IRES-Cre, Jackson Laboratory; stock #027958), Tg(*Slc6a4*-Cre)ET33Gsat (*Sert*-Cre, Jackson Laboratory; MGI: 3836639), *Slc6a3*$^{tm1.1(cre)bkmn}$/J (*Dat*-IRES-Cre, Jackson Laboratory; stock #006660), *Slc6a4*$^{tm1.1(flop)Luo}$/J (*Sert*-IRES-Flp, Jackson Laboratory; stock #034050; Ren et al., 2019), homozygous *Oprk1*$^{tm2.1Kff}$/J (*Oprk1*$^{fl/fl}$, Jackson Laboratory; stock #030076), and Gt(ROSA)$^{26Sortm14(CAG-tdTomato)Hze}$/J (Ai14, Jackson Laboratory; stock #007914) mice were used. All mice (8–18 weeks old) were kept on a C57BL/6J background and group housed on a 12-hr light/dark cycle with food and water *ad libitum*. All procedures complied with animal care standards set forth by the National Institute of Health and were approved by the Stanford University's Administrative Panel on Laboratory Animal Care and Administrative Panel of Biosafety.

METHOD DETAILS

Viral vectors and stereotaxic surgery

AAVs purchased from Stanford Neuroscience Gene Vector and Virus Core: AAVdj-hSyn-Cre-eGFP, AAVdj-hSyn-ΔCre-eGFP, AAVdj-CMV-DIO-eGFP-2A-TeTx, AAVdj-CMV-eGFP-2A-TeTx, AAVdj-CMV-DIO-eGFP, AAVdj-EF1a-DIO-hChR2(H134R)-eYFP, AAVdj-EF1a-DIO-eYFP, AAVdj-EF1a-DIO-mCherry, AAVdj-EF1a-fDIO-eYFP, AAVdj-hSyn-CreON-FlpOFF-eYFP-WPRE, AAVdj-hSyn-CreOFF-FlpON-eYFP-WPRE, AAVdj-hSyn-CreON-FlpON-eYFP-WPRE, AAVdj-hSyn-FLEX-mGFP-2A-Synaptophysin-mRuby, and AAVdj-EF1a-DIO-GCaMP6m. AAV9-hSyn-$GRAB_{5HT}$ 2h (5-HT 3.5) and AAV9-hSyn-$GRAB_{DA}$ 2m (DA 4.4) were purchased from WZ Biosciences (Columbia, MD). All viruses were injected 4–6 · 10^{12} infectious units per mL.

Mice of at least 7 weeks of age were anesthetized with isoflurane (1–2% v/v) and secured in a stereotaxic frame (David Kopf Instruments, Tujunga, CA). Viruses were injected into the DR (AP −4.6; ML ±0; DV −3.1 from skull) or bilaterally into the NAc medial shell (AP +1.1; ML ±0.7; DV −3.6 from dura) at a rate of 150 nL min^{-1} (500 nL total volume) with a borosilicate pipette coupled to a pump-mounted 5 μL Hamilton syringe. Injector pipettes were slowly retracted after a 5 min diffusion period. For optogenetic behavioral experiments, mice were also implanted with optical fibers above the DR (AP −4.6; ML ±0; DV −3.0 from skull) or bilateral NAc (AP +1.1; ML ±1.3; DV −3.1 from dura, 10°). Optical fibers were constructed in-house using 1.25 mm diameter multimode ceramic ferrules (ThorLabs), 200 μm core fiber optic cable with 0.39 numerical aperture (NA) (ThorLabs), and blue dye epoxy (Fiber Instrument Sales). For photometry recordings, optical fibers (Doric Lenses) with 400 μm core and 0.66 NA were unilaterally implanted over the NAc (AP +1.1; ML +0.7; DV −3.6 from dura). Optical fibers were secured to the skull with stainless steel screws (thread size 00–90 × 1/16, Antrin Miniature Specialties), C&B Metabond, and light-cured dental adhesive cement (Geristore A&B paste, DenMat).

For drug microinfusions, a 26-gauge bilateral cannula (P1 Technologies), 3.5 mm in length from the cannula base, was implanted over the NAc (AP +1.1; ML ±0.75; DV −3.1 from dura). Mice that received drug infusions with optogenetic stimulation were implanted with an optical fiber targeting the DR and a guide cannula targeting the NAc in the same surgery. Mice were group housed to recover for 3 weeks before experiments began.

Drug administration

For MOR withdrawal experiments, mice were made MOR dependent with 6 injections of 10–50 mg/kg MOR (Sigma Aldrich, M8777, ip) over a period of 6 days: i.e. 10 mg/kg on day 1, 20 mg/kg on day 2, etc. Mice received a second injection of 50 mg/kg MOR on day 6 (Zhu et al., 2016). Mice were then left undisturbed in homecages for three weeks before behavioral testing or recordings.

For systemic administration of the KOR antagonist Aticaprant, wild-type mice were subjected to protracted withdrawal procedures and then tested in a counterbalanced crossover design. Thirty min before behavioral testing, mice were injected with Aticaprant (3 mg/kg, ip, Med Chem Express) or vehicle (10% ethanol in corn oil, 5 mL/kg) and then

administered the opposite solution before an identical test 48 hours later. This protocol was repeated for the juvenile intruder test, the 3-chamber social preference test, and the CPP posttest. Within-subject comparisons of social behavior and MOR chamber preference after vehicle and Aticaprant injections were made for each subject. Mice that failed to show deficits in at least one social assay during withdrawal were excluded from the study.

For local NAc inhibition of KORs, mice were administered an intra-NAc infusion of norBNI (2.5 μg/hemisphere, Tocris Bioscience) 24 hr prior to behavioral testing. Drugs were infused through an injector cannula coupled to a 5 μL Hamilton syringe using a microinfusion pump (Harvard Apparatus) at a continuous rate of 100 nL min^{-1} to a total volume of 0.3 μL per hemisphere. Injector cannulas were removed 2 min after infusions were complete. Mice were left undisturbed in homecages before behavioral testing. Mice in the experiment displayed in Figures 1L–1O were initially tested for social behavior while in MOR withdrawal. One week later, mice were administered a microinjection of norBNI or saline and then tested in a second round of social assays 24 hr later. Mice in the experiment displayed in Figures 3N–3Q were microinjected with saline 24 hr prior to the first round of sociability testing with optogenetic stimulation. One week later, mice were split into norBNI or saline groups and received a second microinjection of the respective drug into the NAc. 24 hr later all mice were tested in a second round of social assays with optogenetic stimulation in an identical manner to round one.

During fiber photometry experiments, mice were injected with saline or norBNI (10 mg/kg, ip) 24 hr before the final recording. For pharmacology recordings, mice were injected with U-50488 (5 mg/kg, ip, Tocris Bioscience) or MDMA (7.5 mg/kg, NIDA) 5 min into the recording. Some mice administered U-50488 were pretreated with norBNI (10 mg/kg, ip) 24 hr prior to the recording.

Protracted withdrawal behavior

All mice in withdrawal experiments were subjected to a standardized behavioral and drug administration procedure. Mice were initially tested for baseline social behaviors in the juvenile intruder and 3-chamber preference assays. Mice were then administered 6 ascending doses of MOR while confined in a conditioned place preference (CPP) chamber. 24 hr after the last dose of MOR, mice were tested for MOR CPP. Mice were then left undisturbed in homecages for three weeks. After the incubation period, mice were then tested again for social behavior in the same assays. Finally, mice were placed back into the CPP chamber and tested for long-term MOR preference. As much as possible, all behavioral assays were performed blind, without knowledge of the treatment history of the subject.

MOR administration and CPP—To evaluate MOR conditioning effects, mice were allowed to explore a 2-sided CPP chamber with distinct tactile floors and wall patterns (Med Associates Inc.) in a 20 min pretest. The next morning, mice were confined to one side of the chamber for 40 min after receiving an injection of saline. Approximately 4 hr later, mice were confined to the opposite side of the chamber immediately after receiving an injection of MOR, again for 40 min. This procedure was repeated over the next 6 days with the following MOR doses: 10 mg/kg, 20 mg/kg, 30 mg/kg, 40 mg/kg, 50 mg/kg, 50

mg/kg. 24 hr after the 6th conditioning session, mice were allowed to explore both sides of the CPP chamber for 20 min in the first posttest. About 3–4 weeks into protracted MOR withdrawal, mice were tested in a second posttest in an identical manner to the first posttest. Preference was calculated as the percentage of time spent in the MOR-paired side of the chamber during the posttest. MOR-paired sides were assigned in a counterbalanced and unbiased fashion such that the average preference for the MOR-paired side during the pretest was ~50% for all groups.

Juvenile interaction test—Juvenile interaction was performed in the home cage of the test animal as previously described (Gunaydin et al., 2014). Cagemates were temporarily transferred to a holding cage and the test mouse was habituated alone in the home cage for 1 min. After habituation, a novel conspecific juvenile mouse (3–5 weeks of age, strain- and sex-matched) was placed into the home cage for 2 min of free interaction. Sessions were video recorded and analyzed manually post hoc. Interaction time was defined as times during which the test mouse was actively exploring the juvenile mouse as defined by sniffing (including nose, body, and anogenital area), active pursuit, and grooming.

3-chamber sociability test—A 3-chamber sociability test was performed in an arena with three separate chambers as previously described (Kaidanovich-Beilin et al., 2011). On day one, test mice were habituated to the arena with two empty wire mesh cups placed in the two outer chambers for 5 min. Conspecific juvenile mice were also habituated to the mesh cups for 5 min. On day two, the test mouse was placed in the center chamber and a conspecific juvenile (3–5 weeks of age, strain- and sex-matched) was placed into one of the wire mesh cups. After a 2 min habituation, the barriers were raised and the test mouse was allowed to explore freely for a 20 min session. The placement of the juvenile was counterbalanced across sessions. Location of mice was assayed automatically using video tracking software (BIOBSERVE). Sociability was calculated as ((time in juvenile side – time in empty side) / (time in juvenile side + time in empty side)).

3-chamber high-fat food preference test—3-chamber testing was performed as described above, with the exception that a high-fat food pellet was placed under the wire mesh cup instead of a juvenile. The placement of the food pellet was counterbalanced across sessions. Mice were tested once three weeks after injections of MOR or saline. Location of mice was assayed automatically using BIOBSERVE. Preference was again calculated as: ((time in food side – time in empty side) / (time in food side + time in empty side)).

Novel object interaction—The novel object interaction assay was performed in an identical manner as the juvenile interaction assay, with a toy block placed into the animal's home cage. The total time of investigation was again 2 min. Mice were tested once three weeks after injections of MOR or saline.

Open field test—Test mice were placed into the corner of an open field arena (40 × 40 cm) and allowed to move freely for a 10-min session. Time spent in the center (20 × 20 cm) was assayed as a measure of anxiety-like behavior. Total distance traveled and center time was measured automatically using BIOBSERVE. Mice were tested once three weeks after injections of MOR or saline.

Optogenetic stimulation

For optogenetic experiments, optical fibers were connected to a 473 nm laser diode (OEM Laser Systems) through a FC/PC adapter connected to a fiber optic rotary joint commutator (Doric Lenses). BIOBSERVE was programmed to control laser output using a Master-8 pulse stimulator (A.M.P.I.), which delivered 5 ms light pulses at 20 Hz (Walsh et al., 2018). Light output through the fibers was adjusted to ~5 mW for somatic stimulation and ~15 mW for terminal stimulation using a digital power meter console (ThorLabs).

Optogenetic stimulation juvenile interaction test—Juvenile interaction testing was performed as described above but twice in the same subjects, once with optogenetic stimulation and once without. Test mice were connected to a fiber optic patch cord during the habituation period. After habituation, a novel conspecific was placed into the home cage for 2 min of free interaction. The laser remained on for the duration of the session. Interaction time was defined as those times during which the test mouse was actively exploring the juvenile mouse as defined by sniffing (including nose, body, and anogenital area), active pursuit, and grooming. Each test mouse underwent two rounds of the interaction assay, separated by at least 1 hr, with a novel juvenile introduced during each round. Cohorts of mice were counterbalanced for the order of optogenetic stimulation versus no stimulation.

Optogenetic stimulation 3-chamber sociability test—3-chamber testing was performed as described above. Mice had 5 min epochs of the laser being off or on, which were counterbalanced across mice. The placement of the juvenile was also counterbalanced across sessions. For the 3-chamber assay using a high-fat food pellet, the pellet was placed under the wire mesh cup instead of a juvenile. Location of mice was assayed automatically using BIOBSERVE. Sociability was again calculated as: ((time in juvenile side – time in empty side) / (time in juvenile side + time in empty side)).

Optogenetic stimulation real-time place preference—The real-time place preference protocol was conducted as described previously (Walsh et al., 2018) in a rectangular cage with three chambers with similar floors and walls, separated by removable walls. Subjects were placed in the center chamber for 2 min at which point the barriers were lifted and the subject mouse was allowed to freely explore the entire apparatus for 15 min during which it received photostimulation (20 Hz, 5 ms pulses) whenever it entered the designated chamber, which was alternated between each testing session.

Optogenetic stimulation novel object interaction—The novel object interaction assay was performed in an identical manner as the juvenile interaction assay, with a toy block placed into the animal’s home cage. The total time of investigation was again 2 min.

Optogenetic stimulation open field test—Test mice were placed into the corner of an open field arena (40 × 40 cm) and allowed to move freely for an 18-min session. Mice had 3-min epochs of alternating light off or on over 3 cycles, counterbalanced across mice. Time spent in the center (20 × 20 cm) was assayed as a measure of anxiety-like behavior.

Total distance traveled and center time was measured automatically using BIOBSERVE and compared between light on and light off epochs.

Fiber photometry

Fiber photometry was performed as previously described (Heifets et al., 2019; Walsh et al., 2018; Wu et al., 2021). AAVdj-EF1a-DIO-GCaMP6m was injected into the DR with a fiber directed above the DR. AAV9-hSyn-$GRAB_{5HT}$ or AAV9-hSyn-$GRAB_{DA}$ were injected into the NAc medial shell with a fiber directed above. After at least 3 weeks, mice were habituated to the photometry and behavioral setups before any recordings took place. On the test day, mice were connected to patch cables and allowed to habituate alone in the homecage for 2 min. A novel, sex-matched juvenile conspecific was then introduced into the cage for free interaction for 3 min. After the baseline interaction test, all mice were subjected to the MOR administration regimen in their homecages and left undisturbed. Three weeks into protracted withdrawal, the fiber photometry and social test procedure was performed again, identically to the baseline test. One week later, mice treated with MOR were randomly split into saline or norBNI groups and injected ip with the respective compound. 24 hr later, mice were tested in the same fiber photometry and social test procedure. A cohort of homozygous 5-HT KOR knockout mice were prepared and tested in an identical procedure but received no drug injections after MOR administration. Mice used for pharmacology recordings were prepared with $GRAB_{5HT}$ and allowed to recover for at least 3 weeks. 5-HT release was recorded in the homecage during a 5 min baseline. Then the respective drug was injected ip and recordings continued for 40 min.

Data were acquired using Synapse software controlling an RZ5P lock-in amplifier (Tucker-Davis Technologies). GCaMP6m and GRAB sensors were excited by frequency-modulated 465 and 405 nm LEDs (Doric Lenses). Optical signals were band-pass-filtered with a fluorescence mini cube (Doric Lenses) and signals were digitized at 6 kHz. Signal processing was performed with custom scripts in MATLAB (MathWorks). Briefly, signals were de-bleached by fitting with a mono-exponential or bi-exponential decay function and the resulting fluorescence traces were z-scored. Videos were manually analyzed for the first social contact. The first social contact was used in all recordings because of the predicted decrease in sociability during opioid withdrawal. Peristimulus time histograms were constructed by taking the average of 15 sec epochs of fluorescence consisting of 5 sec before and 10 sec after social contact, which was defined as time = 0. Before averaging, each epoch was offset such that the z-score averaged from −5 to −1 sec equaled 0. Peak z-scored fluorescence was determined for each peristimulus time histogram as the maximal z-score value between 0 and +10 sec. Area under the curve was defined as the integral between 0 and +10 sec. Peak z-score and area under the curve were calculated with Prism 9.

Slice electrophysiology

Wild-type mice were unilaterally injected with AAV-CMV-eGFP-p2A-TeTx into the NAc medial shell. Three weeks later, mice were decapitated following deep isoflurane anesthesia. The forebrain was quickly removed and placed in ice cold cutting solution (bubbled with 95%O_2/5%CO_2) consisting (in mM): 228 sucrose, 2.5 KCl, 1.0 NaH_2PO_4, 8 $MgSO_4$, 26 $NaHCO_3$, 20 glucose, and 0.5 $CaCl_2$. The forebrain was then mounted on a cutting platform

and hemisected prior to slicing. Coronal slices (200 μm) containing the NAc were cut with a vibratome (Leica VT1200s) and transferred to a holding chamber containing warmed (30°C, bubbled with 95%O_2/5%CO_2) ASCF consisting of (in mM): 119 NaCl, 2.5 KCl, 1 NaH_2PO_4, 1.3 $MgSO_4$, 26 $NaHCO_3$, 10 glucose, and 2.5 $CaCl_2$. Slices were incubated for 45 min and then kept at room temperature for 1–1.5 hr before being transferred to a fixed recording chamber of an upright microscope (BX51WI, Olympus). Slices were perfused with ACSF (bubbled with 95%O_2/5%CO_2) and maintained at 29–30°C. TeTx infection in the NAc medial shell was identified by eGFP epifluorescence. Whole-cell recordings from neurons in the medial shell were obtained with patch electrodes containing (in mM): 135 $CsMeSO_4$, 10 HEPES, 5 Na-phosphocreatine, 8 NaCl, 0.25 EGTA, 2 $MgCl_2$, 4 Mg-ATP, 0.3 GTP, and 1 spermine (300 mOsM, pH 7.35). Electrode resistances ranged from 2.5–3 MΩ. Series resistance was continually monitored and experiments were discarded if it changed by >20%. Whole-cell voltage clamp recordings were made with a MultiClamp 700B (Molecular Devices). Signals were filtered at 2 KHz and digitized at 10 KHz (National Instruments BNC-209 or Digidata 1320A, Axon Instruments).

IPSCs were evoked with a bipolar electrode fabricated from platinum-iridium wire (A-M systems). To increase the likelihood of stimulating TeTx-infected axons, the stimulating electrode was placed in areas of high eGFP epifluorescence. Whole-cell recordings were made from neurons in the infected area in close proximity (<100 μm) to the stimulating electrode. This arrangement was also applied to recordings from uninfected slices. Evoked and spontaneous IPSCs were recorded at a holding potential of 5 mV in the presence of 10 μM NBQX, 50 μM D-AP5, and 5 μM CGP55845 (all from Tocris Bioscience). IPSCs were evoked at 0.2 Hz with stimulation intensities ranging from 10–50 μA. To generate input-output graphs each point on the graphs represents the average amplitude of ten consecutive IPSCs recorded at each stimulation intensity. sIPSCs were recorded “gap-free” for 5 min and data were analyzed with MiniAnalysis software (Synaptosoft). Recordings performed in the TeTx-infected hemisphere were compared to those in the uninfected hemisphere.

Histology

Mice were anesthetized with isoflurane and perfused transcardially with 1X PBS followed by 4% paraformaldehyde in PBS, pH 7.4. Brains were extracted and post-fixed overnight in the same fixative. Brains were sectioned at 40 μm on a vibratome and collected in PBS. Free-floating sections were washed three times in PBS for 10 min at room temperature and then incubated in PBS with 0.5% Triton X-100, 10% normal goat serum, and 0.2% bovine serum albumin (BSA) for 1 hr. After a 5 min wash in PBS, sections were next incubated in primary antibodies rabbit anti-TPH2 (1:1000, Novus Biologicals, NB100–74555), mouse anti-TH (1:1000, Millipore, MAB318), rat anti-mCherry (1:1000, Millipore, MAB131873), or chicken anti-GFP (1:1000, Aves Labs, GFP-1010) in carrier solution containing 0.5% Triton X-100, 1% normal goat serum, and 0.2% BSA in PBS shaking at room temperature for 24 hr. After four 10 min washes in PBS, sections were incubated in species-specific secondary antibodies Alexa Fluor 488, 594, or 647 (1:750, Invitrogen, Carlsbad, CA, A-11039, A-11058, and A-31573) in carrier solution for 2 hr at room temperature. Finally, sections were washed four times for 10 min in PBS, mounted onto SuperFrost Plus glass slides, and coverslipped with Fluoromount-G with DAPI (Southern Biotech, Birmingham,

AL, 0100–20). Fluorescent images were collected on a Nikon A1 confocal microscope or a Keyence BZ-X800 fluorescence microscope.

Fluorescence *in situ* hybridization

For examination of gene expression in the DR and VTA, wild-type brains were flash frozen in isopentane on dry ice, sectioned on a cryostat at 16 μm, and processed for fluorescence *in situ* hybridization (FISH) with the RNAscope Multiplex Fluorescent v2 assay according to the manufacturer's guidelines (Advanced Cell Diagnostics). Transcripts examined were *Slc6a4 (Sert)* (ACDBio cat# 315851), *Slc6a3* (*Dat)* (ACDBio cat# 315441), and *Oprk1* (ACDBio cat# 316111). Slides were coverslipped with Fluoromount-G with DAPI (Southern Biotech, 0100–20) and stored at 4°C in the dark before imaging. For verification of *Oprk1* deletion, midbrain sections from *Sert*-Cre and *Dat*-Cre mice crossed to *Oprk1*$^{fl/fl}$ mice were processed as described above. Cre- mice from the same litters served as wild-type controls. For analysis of NAc-projecting DR neurons, wild-type mice were bilaterally injected with 200 nL of CTB-647 (4 μg/μL) into the NAc and sacrificed 14 days later. To preserve CTB fluorescence, the only modification to the RNAscope protocol was the application of protease III for 10 min, as opposed to protease IV for 30 min. Fluorescent images were collected on a Nikon A1 confocal microscope. Each image was acquired using identical pinhole, gain, offset, and laser settings (1024 × 1024 pixels). Cells were counted and co-localization was measured using custom macros in Fiji (Schindelin et al., 2012). For measuring *Oprk1* deletion, analysis was restricted to regions of interest (ROIs) specifically within the *Sert* or *Dat* cell populations. The mean pixel intensity of *Oprk1* within these ROIs was calculated. The number of *Sert* or *Dat* neurons expressing *Oprk1* was also calculated and normalized to the total number of *Sert* or *Dat* neurons for each section and averaged for each subject.

QUANTIFICATION AND STATISTICAL ANALYSIS

Full statistical information is provided in Table S1. Investigators were blinded to the manipulations that experimental subjects had received during behavioral testing, recordings, and data analysis. All behavioral data were analyzed and graphed with GraphPad Prism 9. All photometry data were processed and analyzed in MATLAB. Data distribution and variance were tested using Shapiro-Wilk normality tests. Normally distributed data were analyzed by unpaired, two-tailed t-tests, or one- or two-factor repeated measures ANOVA with *post-hoc* Sidak or Tukey correction. When normal distributions were not assumed, the Mann-Whitney rank test was performed for between-group comparisons. Paired comparisons were performed when appropriate. Differences were considered significant when $p < 0.05$. All pooled data are expressed as mean ± SEM.

TABLE FOR AUTHOR TO COMPLETE

Please upload the completed table as a separate document. **Please do not add subheadings to the key resources table.** If you wish to make an entry that does not fall into one of the subheadings below, please contact your handling editor. **Any subheadings not relevant to your study can be skipped.** (**NOTE:** For authors publishing in Cell Genomics, Cell Reports

Medicine, Current Biology, and Med, please note that references within the KRT should be in numbered style rather than Harvard.)

Supplementary Material

Refer to Web version on PubMed Central for supplementary material.

ACKNOWLEDGEMENTS

We thank Alexandra Groome and Lara Taniguchi for support with animal breeding and histology and the Wu Tsai Neurosciences Institute Gene Vector and Virus Core for providing viruses. We also thank Dr. Sarah Melzer for advice on FISH and Dr. Jinhee Baek for assistance with histology and fiber photometry surgery. This work was supported by grants from the Stanford University Wu Tsai Neurosciences Institute (to R.C.M.), the UCSF Dolby Family Center for Mood Disorders (to R.C.M.), NIH grants P50DA042012 (to R.C.M.), K08MH123791 (to N.E.), K99DA056573, and T32DA035165 (to M.B.P.), NSF and HHMI Gilliam Fellowships (to D.F.C.P. and R.C.M.), a Brain & Behavior Research Foundation Young Investigator Grant, a Burroughs Wellcome Fund Career Award for Medical Scientists, a Stanford Society of Physician Scholars Research Grant, and the Simons Foundation Bridge to Independence Award (to N.E.).

REFERENCES

Abbott PJ (2009). A review of the community reinforcement approach in the treatment of opioid dependence. J Psychoactive Drugs 41, 379–385. 10.1080/02791072.2009.10399776. [PubMed: 20235445]

Abraham AD, Casello SM, Schattauer SS, Wong BA, Mizuno GO, Mahe K, Tian L, Land BB, and Chavkin C (2021). Release of endogenous dynorphin opioids in the prefrontal cortex disrupts cognition. Neuropsychopharmacology 46, 2330–2339. 10.1038/s41386-021-01168-2. [PubMed: 34545197]

Abraham AD, Casello SM, Land BB, and Chavkin C (2022). Optogenetic stimulation of dynorphinergic neurons within the dorsal raphe activate kappa opioid receptors in the ventral tegmental area and ablation of dorsal raphe prodynorphin or kappa receptors in dopamine neurons blocks stress potentiation of cocaine reward. Addiction Neuroscience 1, 100005. 10.1016/j.addicn.2022.100005. [PubMed: 36176476]

Al-Hasani R, McCall JG, Shin G, Gomez AM, Schmitz GP, Bernardi JM, Pyo CO, Park SI, Marcinkiewcz CM, Crowley NA, et al. (2015). Distinct Subpopulations of Nucleus Accumbens Dynorphin Neurons Drive Aversion and Reward. Neuron 87, 1063–1077. 10.1016/j.neuron.2015.08.019. [PubMed: 26335648]

Bart G (2012). Maintenance medication for opiate addiction: the foundation of recovery. J Addict Dis 31, 207–225. 10.1080/10550887.2012.694598. [PubMed: 22873183]

Beardsley PM, Howard JL, Shelton KL, and Carroll FI (2005). Differential effects of the novel kappa opioid receptor antagonist, JDTic, on reinstatement of cocaine-seeking induced by footshock stressors vs cocaine primes and its antidepressant-like effects in rats. Psychopharmacology (Berl) 183, 118–126. 10.1007/s00213-005-0167-4. [PubMed: 16184376]

Blanco C, and Volkow ND (2019). Management of opioid use disorder in the USA: present status and future directions. Lancet 393, 1760–1772. 10.1016/S0140-6736(18)33078-2. [PubMed: 30878228]

Bravo IM, Luster BR, Flanigan ME, Perez PJ, Cogan ES, Schmidt KT, and McElligott ZA (2020). Divergent behavioral responses in protracted opioid withdrawal in male and female C57BL/6J mice. Eur J Neurosci 51, 742–754. 10.1111/ejn.14580. [PubMed: 31544297]

Bruchas MR, Land BB, and Chavkin C (2010). The dynorphin/kappa opioid system as a modulator of stress-induced and pro-addictive behaviors. Brain Res 1314, 44–55. 10.1016/j.brainres.2009.08.062. [PubMed: 19716811]

Bruchas MR, Schindler AG, Shankar H, Messinger DI, Miyatake M, Land BB, Lemos JC, Hagan CE, Neumaier JF, Quintana A, et al. (2011). Selective p38alpha MAPK deletion in serotonergic neurons produces stress resilience in models of depression and addiction. Neuron 71, 498–511. 10.1016/j.neuron.2011.06.011. [PubMed: 21835346]

Bruchas MR, Yang T, Schreiber S, Defino M, Kwan SC, Li S, and Chavkin C (2007). Long-acting kappa opioid antagonists disrupt receptor signaling and produce noncompetitive effects by activating c-Jun N-terminal kinase. J Biol Chem 282, 29803–29811. 10.1074/jbc.M705540200. [PubMed: 17702750]

Cardozo Pinto DF, Yang H, Pollak Dorocic I, de Jong JW, Han VJ, Peck JR, Zhu Y, Liu C, Beier KT, Smidt MP, et al. (2019). Characterization of transgenic mouse models targeting neuromodulatory systems reveals organizational principles of the dorsal raphe. Nat Commun 10, 4633. 10.1038/s41467-019-12392-2. [PubMed: 31604921]

Carlezon WA Jr., Thome J, Olson VG, Lane-Ladd SB, Brodkin ES, Hiroi N, Duman RS, Neve RL, and Nestler EJ (1998). Regulation of cocaine reward by CREB. Science 282, 2272–2275. DOI: 10.1126/science.282.5397.2272. [PubMed: 9856954]

Castro DC, and Berridge KC (2014). Opioid hedonic hotspot in nucleus accumbens shell: mu, delta, and kappa maps for enhancement of sweetness “liking” and “wanting”. J Neurosci 34, 4239–4250. 10.1523/JNEUROSCI.4458-13.2014. [PubMed: 24647944]

Castro DC, and Bruchas MR (2019). A Motivational and Neuropeptidergic Hub: Anatomical and Functional Diversity within the Nucleus Accumbens Shell. Neuron 102, 529–552. 10.1016/j.neuron.2019.03.003. [PubMed: 31071288]

Castro DC, Oswell CS, Zhang ET, Pedersen CE, Piantadosi SC, Rossi MA, Hunker AC, Guglin A, Moron JA, Zweifel LS, et al. (2021). An endogenous opioid circuit determines state-dependent reward consumption. Nature 598, 646–651. 10.1038/s41586-021-04013-0. [PubMed: 34646022]

Chartoff E, Sawyer A, Rachlin A, Potter D, Pliakas A, and Carlezon WA (2012). Blockade of kappa opioid receptors attenuates the development of depressive-like behaviors induced by cocaine withdrawal in rats. Neuropharmacology 62, 167–176. 10.1016/j.neuropharm.2011.06.014. [PubMed: 21736885]

Cho JR, Treweek JB, Robinson JE, Xiao C, Bremner LR, Greenbaum A, and Gradinaru V (2017). Dorsal Raphe Dopamine Neurons Modulate Arousal and Promote Wakefulness by Salient Stimuli. Neuron 94, 1205–1219 e1208. 10.1016/j.neuron.2017.05.020. [PubMed: 28602690]

Christie NC (2021). The role of social isolation in opioid addiction. Soc Cogn Affect Neurosci 16, 645–656. 10.1093/scan/nsab029. [PubMed: 33681992]

Crowley NA, and Kash TL (2015). Kappa opioid receptor signaling in the brain: Circuitry and implications for treatment. Prog Neuropsychopharmacol Biol Psychiatry 62, 51–60. 10.1016/j.pnpbp.2015.01.001. [PubMed: 25592680]

Dai B, Sun F, Tong X, Ding Y, Kuang A, Osakada T, Li Y, and Lin D (2022). Responses and functions of dopamine in the nucleus accumbens core during social behaviors. Cell Reports 40, 111246. 10.1016/j.celrep.2022.111246. [PubMed: 36001967]

Darcq E, and Kieffer BL (2018). Opioid receptors: drivers to addiction? Nat Rev Neurosci 19, 499–514. 10.1038/s41583-018-0028-x. [PubMed: 29934561]

DePaoli AM, Hurley KM, Yasada K, Reisine T, and Bell G (1994). Distribution of kappa opioid receptor mRNA in adult mouse brain: an in situ hybridization histochemistry study. Mol Cell Neurosci 5, 327–335. 10.1006/mcne.1994.1039. [PubMed: 7804602]

Dolen G, Darvishzadeh A, Huang KW, and Malenka RC (2013). Social reward requires coordinated activity of nucleus accumbens oxytocin and serotonin. Nature 501, 179–184. 10.1038/nature12518. [PubMed: 24025838]

Ehrich JM, Messinger DI, Knakal CR, Kuhar JR, Schattauer SS, Bruchas MR, Zweifel LS, Kieffer BL, Phillips PE, and Chavkin C (2015). Kappa Opioid Receptor-Induced Aversion Requires p38 MAPK Activation in VTA Dopamine Neurons. J Neurosci 35, 12917–12931. 10.1523/JNEUROSCI.2444-15.2015. [PubMed: 26377476]

Epstein DH, Willner-Reid J, Vahabzadeh M, Mezghanni M, Lin JL, and Preston KL (2009). Real-time electronic diary reports of cue exposure and mood in the hours before cocaine and heroin craving and use. Arch Gen Psychiatry 66, 88–94. doi:10.1001/archgenpsychiatry.2008.509. [PubMed: 19124692]

Fellinger L, Jo YS, Hunker AC, Soden ME, Elum J, Juarez B, and Zweifel LS (2021). A midbrain dynorphin circuit promotes threat generalization. Curr Biol 31, 4388–4396 e4385. 10.1016/j.cub.2021.07.047. [PubMed: 34388372]

Florence C, Luo F, and Rice K (2021). The economic burden of opioid use disorder and fatal opioid overdose in the United States, 2017. Drug Alcohol Depend 218, 108350. 10.1016/j.drugalcdep.2020.108350. [PubMed: 33121867]

Ford CP, Mark GP, and Williams JT (2006). Properties and opioid inhibition of mesolimbic dopamine neurons vary according to target location. J Neurosci 26, 2788–2797. 10.1523/JNEUROSCI.4331-05.2006. [PubMed: 16525058]

Goeldner C, Lutz PE, Darcq E, Halter T, Clesse D, Ouagazzal AM, and Kieffer BL (2011). Impaired emotional-like behavior and serotonergic function during protracted abstinence from chronic morphine. Biol Psychiatry 69, 236–244. 10.1016/j.biopsych.2010.08.021. [PubMed: 20947067]

Graziane NM, Polter AM, Briand LA, Pierce RC, and Kauer JA (2013). Kappa opioid receptors regulate stress-induced cocaine seeking and synaptic plasticity. Neuron 77, 942–954. 10.1016/j.neuron.2012.12.034. [PubMed: 23473323]

Green AR, Mechan AO, Elliott JM, O'Shea E, and Colado MI (2003). The pharmacology and clinical pharmacology of 3,4-methylenedioxymethamphetamine (MDMA, "ecstasy"). Pharmacol Rev 55, 463–508. 10.1124/pr.55.3.3. [PubMed: 12869661]

Gunaydin LA, Grosenick L, Finkelstein JC, Kauvar IV, Fenno LE, Adhikari A, Lammel S, Mirzabekov JJ, Airan RD, Zalocusky KA, et al. (2014). Natural neural projection dynamics underlying social behavior. Cell 157, 1535–1551. 10.1016/j.cell.2014.05.017. [PubMed: 24949967]

Harris GC, and Aston-Jones G (2001). Augmented accumbal serotonin levels decrease the preference for a morphine associated environment during withdrawal. Neuropsychopharmacology 24, 75–85. 10.1016/S0893-133X(00)00184-6. [PubMed: 11106878]

Heifets BD, and Malenka RC (2021). Better living through chemistry: MDMA's prosocial mechanism as a starting point for improved therapeutics. Neuropsychopharmacology 46, 261. 10.1038/s41386-020-00803-8. [PubMed: 32792684]

Heifets BD, Salgado JS, Taylor MD, Hoerbelt P, Cardozo Pinto DF, Steinberg EE, Walsh JJ, Sze JY, and Malenka RC (2019). Distinct neural mechanisms for the prosocial and rewarding properties of MDMA. Sci Transl Med 11, 522. DOI: 10.1126/scitranslmed.aaw6435.

Heilig M, Epstein DH, Nader MA, and Shaham Y (2016). Time to connect: bringing social context into addiction neuroscience. Nat Rev Neurosci 17, 592–599. 10.1038/nrn.2016.67. [PubMed: 27277868]

Huang KW, Ochandarena NE, Philson AC, Hyun M, Birnbaum JE, Cicconet M, and Sabatini BL (2019). Molecular and anatomical organization of the dorsal raphe nucleus. Elife 8, e46464. 10.7554/eLife.46464. [PubMed: 31411560]

Humphreys K, Shover CL, Andrews CM, Bohnert ASB, Brandeau ML, Caulkins JP, Chen JH, Cuellar MF, Hurd YL, Juurlink DN, et al. (2022). Responding to the opioid crisis in North America and beyond: recommendations of the Stanford-Lancet Commission. Lancet 399, 555–604. 10.1016/S0140-6736(21)02252-2. [PubMed: 35122753]

Hung LW, Neuner S, Polepalli JS, Beier KT, Wright M, Walsh JJ, Lewis EM, Luo L, Deisseroth K, Dolen G, et al. (2017). Gating of social reward by oxytocin in the ventral tegmental area. Science 357, 1406–1411. DOI: 10.1126/science.aan4994. [PubMed: 28963257]

Kaidanovich-Beilin O, Lipina T, Vukobradovic I, Roder J, and Woodgett JR (2011). Assessment of social interaction behaviors. J Vis Exp Feb 25; (48): 2473. doi: 10.3791/2473. [PubMed: 21403628]

Keefe PR (2021). Empire of pain : the secret history of the Sackler dynasty, First edition. edn (New York: Doubleday).

Kim JC, Cook MN, Carey MR, Shen C, Regehr WG, and Dymecki SM (2009). Linking genetically defined neurons to behavior through a broadly applicable silencing allele. Neuron 63, 305–315. 10.1016/j.neuron.2009.07.010. [PubMed: 19679071]

Koob GF (2008). A role for brain stress systems in addiction. Neuron 59, 11–34. 10.1016/j.neuron.2008.06.012. [PubMed: 18614026]

Kosten TR, and Petrakis IL (2021). The Hidden Epidemic of Opioid Overdoses During the Coronavirus Disease 2019 Pandemic. JAMA Psychiatry 78, 585–586. doi:10.1001/jamapsychiatry.2020.4148. [PubMed: 33377967]

Krystal AD, Pizzagalli DA, Smoski M, Mathew SJ, Nurnberger J, Lisanby SH, Iosifescu D, Murrough JW, Yang H, Weiner RD, et al. (2020). A randomized proof-of-mechanism trial applying the 'fast-fail' approach to evaluating κ-opioid antagonism as a treatment for anhedonia. Nature Medicine 26, 760–768. 10.1038/s41591-020-0806-7.

Lalanne L, Ayranci G, Filliol D, Gaveriaux-Ruff C, Befort K, Kieffer BL, and Lutz PE (2017). Kappa opioid receptor antagonism and chronic antidepressant treatment have beneficial activities on social interactions and grooming deficits during heroin abstinence. Addict Biol 22, 1010–1021. 10.1111/adb.12392. [PubMed: 27001273]

Lalanne L, Ayranci G, Kieffer BL, and Lutz PE (2014). The kappa opioid receptor: from addiction to depression, and back. Front Psychiatry 5, 170. 10.3389/fpsyt.2014.00170. [PubMed: 25538632]

Land BB, Bruchas MR, Lemos JC, Xu M, Melief EJ, and Chavkin C (2008). The dysphoric component of stress is encoded by activation of the dynorphin kappa-opioid system. J Neurosci 28, 407–414. 10.1523/JNEUROSCI.4458-07.2008. [PubMed: 18184783]

Land BB, Bruchas MR, Schattauer S, Giardino WJ, Aita M, Messinger D, Hnasko TS, Palmiter RD, and Chavkin C (2009). Activation of the kappa opioid receptor in the dorsal raphe nucleus mediates the aversive effects of stress and reinstates drug seeking. Proc Natl Acad Sci U S A 106, 19168–19173. 10.1073/pnas.0910705106. [PubMed: 19864633]

Lein ES, Hawrylycz MJ, Ao N, Ayres M, Bensinger A, Bernard A, Boe AF, Boguski MS, Brockway KS, Byrnes EJ et al. (2007). Genome-wide atlas of gene expression in the adult mouse brain. Nature 11, 168–174. 10.1038/nature05453.

Lembke A (2016). Drug dealer, MD : how doctors were duped, patients got hooked, and why it's so hard to stop (Baltimore: Johns Hopkins University Press).

Lemos JC, Roth CA, Messinger DI, Gill HK, Phillips PE, and Chavkin C (2012). Repeated stress dysregulates kappa-opioid receptor signaling in the dorsal raphe through a p38alpha MAPK-dependent mechanism. J Neurosci 32, 12325–12336. 10.1523/JNEUROSCI.2053-12.2012. [PubMed: 22956823]

Lin R, Liang J, Wang R, Yan T, Zhou Y, Liu Y, Feng Q, Sun F, Li Y, Li A, et al. (2020). The Raphe Dopamine System Controls the Expression of Incentive Memory. Neuron 106, 498–514 e498. 10.1016/j.neuron.2020.02.009. [PubMed: 32145184]

Lutz PE, Ayranci G, Chu-Sin-Chung P, Matifas A, Koebel P, Filliol D, Befort K, Ouagazzal AM, and Kieffer BL (2014). Distinct mu, delta, and kappa opioid receptor mechanisms underlie low sociability and depressive-like behaviors during heroin abstinence. Neuropsychopharmacology 39, 2694–2705. 10.1038/npp.2014.126. [PubMed: 24874714]

Lutz PE, and Kieffer BL (2013). Opioid receptors: distinct roles in mood disorders. Trends Neurosci 36, 195–206. 10.1016/j.tins.2012.11.002. [PubMed: 23219016]

Lutz PE, Pradhan AA, Goeldner C, and Kieffer BL (2011). Sequential and opposing alterations of 5-HT(1A) receptor function during withdrawal from chronic morphine. Eur Neuropsychopharmacol 21, 835–840. 10.1016/j.euroneuro.2011.02.002. [PubMed: 21402471]

Mague SD, Pliakas AM, Todtenkopf MS, Tomasiewicz HC, Zhang Y, Stevens WC Jr., Jones RM, Portoghese PS, and Carlezon WA Jr. (2003). Antidepressant-like effects of kappa-opioid receptor antagonists in the forced swim test in rats. J Pharmacol Exp Ther 305, 323–330. 10.1124/jpet.102.046433. [PubMed: 12649385]

Marsden J, Darke S, Hall W, Hickman M, Holmes J, Humphreys K, Neale J, Tucker J, and West R (2020). Mitigating and learning from the impact of COVID-19 infection on addictive disorders. Addiction 115, 1007–1010. 10.1111/add.15080. [PubMed: 32250482]

Massaly N, Copits BA, Wilson-Poe AR, Hipolito L, Markovic T, Yoon HJ, Liu S, Walicki MC, Bhatti DL, Sirohi S, et al. (2019). Pain-Induced Negative Affect Is Mediated via Recruitment of The Nucleus Accumbens Kappa Opioid System. Neuron 102, 564–573 e566. 10.1016/j.neuron.2019.02.029. [PubMed: 30878290]

Massaly N, Moron JA, and Al-Hasani R (2016). A Trigger for Opioid Misuse: Chronic Pain and Stress Dysregulate the Mesolimbic Pathway and Kappa Opioid System. Front Neurosci 10, 480. 10.3389/fnins.2016.00480. [PubMed: 27872581]

Matthews GA, Nieh EH, Vander Weele CM, Halbert SA, Pradhan RV, Yosafat AS, Glober GF, Izadmehr EM, Thomas RE, Lacy GD, et al. (2016). Dorsal Raphe Dopamine Neurons Represent

the Experience of Social Isolation. Cell 164, 617–631. 10.1016/j.cell.2015.12.040. [PubMed: 26871628]

McLaughlin JP, Li S, Valdez J, Chavkin TA, and Chavkin C (2006). Social defeat stress-induced behavioral responses are mediated by the endogenous kappa opioid system. Neuropsychopharmacology 31, 1241–1248. 10.1038/sj.npp.1300872. [PubMed: 16123746]

McLaughlin JP, Marton-Popovici M, and Chavkin C (2003). Kappa opioid receptor antagonism and prodynorphin gene disruption block stress-induced behavioral responses. J Neurosci 23, 5674–5683. 10.1523/JNEUROSCI.23-13-05674.2003. [PubMed: 12843270]

Melief EJ, Miyatake M, Bruchas MR, and Chavkin C (2010). Ligand-directed c-Jun N-terminal kinase activation disrupts opioid receptor signaling. Proc Natl Acad Sci U S A 107, 11608–11613. 10.1073/pnas.1000751107. [PubMed: 20534436]

Nunes EV, and Levin FR (2006). Treating depression in substance abusers. Curr Psychiatry Rep 8, 363–370. 10.1007/s11920-006-0037-8. [PubMed: 16968616]

Okaty BW, Sturrock N, Escobedo Lozoya Y, Chang Y, Senft RA, Lyon KA, Alekseyenko OV, and Dymecki SM (2020). A single-cell transcriptomic and anatomic atlas of mouse dorsal raphe Pet1 neurons. Elife 9, e55523. 10.7554/eLife.55523. [PubMed: 32568072]

Pantazis CB, Gonzalez LA, Tunstall BJ, Carmack SA, Koob GF, and Vendruscolo LF (2021). Cues conditioned to withdrawal and negative reinforcement: Neglected but key motivational elements driving opioid addiction. Sci Adv 7, eabf0364. DOI: 10.1126/sciadv.abf0364. [PubMed: 33827822]

Pirino BE, Spodnick MB, Gargiulo AT, Curtis GR, Barson JR, and Karkhanis AN (2020). Kappa-opioid receptor-dependent changes in dopamine and anxiety-like or approach-avoidance behavior occur differentially across the nucleus accumbens shell rostro-caudal axis. Neuropharmacology 181, 108341. 10.1016/j.neuropharm.2020.108341. [PubMed: 33011200]

Polter AM, Barcomb K, Chen RW, Dingess PM, Graziane NM, Brown TE, and Kauer JA (2017). Constitutive activation of kappa opioid receptors at ventral tegmental area inhibitory synapses following acute stress. Elife 6, e23785. 10.7554/eLife.23785. [PubMed: 28402252]

Polter AM, Bishop RA, Briand LA, Graziane NM, Pierce RC, and Kauer JA (2014). Poststress block of kappa opioid receptors rescues long-term potentiation of inhibitory synapses and prevents reinstatement of cocaine seeking. Biol Psychiatry 76, 785–793. 10.1016/j.biopsych.2014.04.019. [PubMed: 24957331]

Redila VA, and Chavkin C (2008). Stress-induced reinstatement of cocaine seeking is mediated by the kappa opioid system. Psychopharmacology (Berl) 200, 59–70. 10.1007/s00213-008-1122-y. [PubMed: 18575850]

Ren J, Isakova A, Friedmann D, Zeng J, Grutzner SM, Pun A, Zhao GQ, Kolluru SS, Wang R, Lin R, et al. (2019). Single-cell transcriptomes and whole-brain projections of serotonin neurons in the mouse dorsal and median raphe nuclei. Elife 8, e49424. 10.7554/eLife.49424. [PubMed: 31647409]

Resendez SL, Keyes PC, Day JJ, Hambro C, Austin CJ, Maina FK, Eidson LN, Porter-Stransky KA, Nevarez N, McLean JW, et al. (2016). Dopamine and opioid systems interact within the nucleus accumbens to maintain monogamous pair bonds. Elife 5, e15325. 10.7554/eLife.15325. [PubMed: 27371827]

Resendez SL, Kuhnmuench M, Krzywosinski T, and Aragona BJ (2012). kappa-Opioid receptors within the nucleus accumbens shell mediate pair bond maintenance. J Neurosci 32, 6771–6784. 10.1523/JNEUROSCI.5779-11.2012. [PubMed: 22593047]

Robinson TE, and Berridge KC (2003). Addiction. Annu Rev Psychol 54, 25–53. 10.1146/annurev.psych.54.101601.145237. [PubMed: 12185211]

Robles CF, McMackin MZ, Campi KL, Doig IE, Takahashi EY, Pride MC, and Trainor BC (2014). Effects of kappa opioid receptors on conditioned place aversion and social interaction in males and females. Behav Brain Res 262, 84–93. 10.1016/j.bbr.2014.01.003. [PubMed: 24445073]

Schindelin J, Arganda-Carreras I, Frise E, Kaynig V, Longair M, Pietzsch T, Preibisch S, Rueden C, Saalfeld S, Schmid B, et al. (2012). Fiji: an open-source platform for biological-image analysis. Nat Methods 9, 676–682. 10.1038/nmeth.2019. [PubMed: 22743772]

Schindler AG, Messinger DI, Smith JS, Shankar H, Gustin RM, Schattauer SS, Lemos JC, Chavkin NW, Hagan CE, Neumaier JF, et al. (2012). Stress produces aversion and potentiates cocaine reward by releasing endogenous dynorphins in the ventral striatum to locally stimulate serotonin reuptake. J Neurosci 32, 17582–17596. 10.1523/JNEUROSCI.3220-12.2012. [PubMed: 23223282]

Schlosburg JE, Whitfield TW Jr., Park PE, Crawford EF, George O, Vendruscolo LF, and Koob GF (2013). Long-term antagonism of kappa opioid receptors prevents escalation of and increased motivation for heroin intake. J Neurosci 33, 19384–19392. 10.1523/JNEUROSCI.1979-13.2013. [PubMed: 24305833]

Shirayama Y, Ishida H, Iwata M, Hazama GI, Kawahara R, and Duman RS (2004). Stress increases dynorphin immunoreactivity in limbic brain regions and dynorphin antagonism produces antidepressant-like effects. J Neurochem 90, 1258–1268. 10.1111/j.1471-4159.2004.02589.x. [PubMed: 15312181]

Spanagel R, Herz A, and Shippenberg TS (1992). Opposing tonically active endogenous opioid systems modulate the mesolimbic dopaminergic pathway. Proc Natl Acad Sci U S A 89, 2046–2050. 10.1073/pnas.89.6.2046. [PubMed: 1347943]

Strang J, Volkow ND, Degenhardt L, Hickman M, Johnson K, Koob GF, Marshall BDL, Tyndall M, and Walsh SL (2020). Opioid use disorder. Nat Rev Dis Primers 6, 3. 10.1038/s41572-019-0137-5. [PubMed: 31919349]

Sun F, Zhou J, Dai B, Qian T, Zeng J, Li X, Zhuo Y, Zhang Y, Wang Y, Qian C, et al. (2020). Next-generation GRAB sensors for monitoring dopaminergic activity in vivo. Nat Methods 17, 1156–1166. 10.1038/s41592-020-00981-9. [PubMed: 33087905]

Svingos AL, Chavkin C, Colago EE, and Pickel VM (2001). Major coexpression of kappa-opioid receptors and the dopamine transporter in nucleus accumbens axonal profiles. Synapse 42, 185–192. 10.1002/syn.10005. [PubMed: 11746715]

Tao R, and Auerbach SB (2002). Opioid receptor subtypes differentially modulate serotonin efflux in the rat central nervous system. J Pharmacol Exp Ther 303, 549–556. 10.1124/jpet.102.037861. [PubMed: 12388635]

Tao R, Ma Z, and Auerbach SB (1998). Alteration in regulation of serotonin release in rat dorsal raphe nucleus after prolonged exposure to morphine. J Pharmacol Exp Ther 286, 481–488. https://jpet.aspetjournals.org/content/286/1/481.long. [PubMed: 9655893]

Tejeda HA, and Bonci A (2019). Dynorphin/kappa-opioid receptor control of dopamine dynamics: Implications for negative affective states and psychiatric disorders. Brain Res 1713, 91–101. 10.1016/j.brainres.2018.09.023. [PubMed: 30244022]

Tejeda HA, Shippenberg TS, and Henriksson R (2012). The dynorphin/kappa-opioid receptor system and its role in psychiatric disorders. Cell Mol Life Sci 69, 857–896. 10.1007/s00018-011-0844-x. [PubMed: 22002579]

Van't Veer A, and Carlezon WA Jr. (2013). Role of kappa-opioid receptors in stress and anxiety-related behavior. Psychopharmacology (Berl) 229, 435–452. 10.1007/s00213-013-3195-5. [PubMed: 23836029]

van den Pol AN (2012). Neuropeptide transmission in brain circuits. Neuron 76, 98–115. 10.1016/j.neuron.2012.09.014. [PubMed: 23040809]

Volkow ND (2020). Collision of the COVID-19 and Addiction Epidemics. Ann Intern Med 173, 61–62. 10.7326/M20-1212. [PubMed: 32240293]

Volkow ND, and Blanco C (2021). The changing opioid crisis: development, challenges and opportunities. Mol Psychiatry 26, 218–233. 10.1038/s41380-020-0661-4. [PubMed: 32020048]

Walsh JJ, Christoffel DJ, Heifets BD, Ben-Dor GA, Selimbeyoglu A, Hung LW, Deisseroth K, and Malenka RC (2018). 5-HT release in nucleus accumbens rescues social deficits in mouse autism model. Nature 560, 589–594. 10.1038/s41586-018-0416-4. [PubMed: 30089910]

Walsh JJ, Llorach P, Cardozo Pinto DF, Wenderski W, Christoffel DJ, Salgado JS, Heifets BD, Crabtree GR, and Malenka RC (2021). Systemic enhancement of serotonin signaling reverses social deficits in multiple mouse models for ASD. Neuropsychopharmacology 46, 2000–2010. 10.1038/s41386-021-01091-6. [PubMed: 34239048]

Wan J, Peng W, Li X, Qian T, Song K, Zeng J, Deng F, Hao S, Feng J, Zhang P, et al. (2021). A genetically encoded sensor for measuring serotonin dynamics. Nat Neurosci 24, 746–752. 10.1038/s41593-021-00823-7. [PubMed: 33821000]

Wang J, Li J, Yang Q, Xie YK, Wen YL, Xu ZZ, Li Y, Xu T, Wu ZY, Duan S, et al. (2021). Basal forebrain mediates prosocial behavior via disinhibition of midbrain dopamine neurons. Proc Natl Acad Sci U S A 118, e2019295118. 10.1073/pnas.2019295118. [PubMed: 33563763]

Wee S, and Koob GF (2010). The role of the dynorphin-kappa opioid system in the reinforcing effects of drugs of abuse. Psychopharmacology (Berl) 210, 121–135. 10.1007/s00213-010-1825-8. [PubMed: 20352414]

Welsch L, Bailly J, Darcq E, and Kieffer BL (2020). The Negative Affect of Protracted Opioid Abstinence: Progress and Perspectives From Rodent Models. Biol Psychiatry 87, 54–63. 10.1016/j.biopsych.2019.07.027. [PubMed: 31521334]

Williams AV, Laman-Maharg A, Armstrong CV, Ramos-Maciel S, Minie VA, and Trainor BC (2018). Acute inhibition of kappa opioid receptors before stress blocks depression-like behaviors in California mice. Prog Neuropsychopharmacol Biol Psychiatry 86, 166–174. 10.1016/j.pnpbp.2018.06.001. [PubMed: 29879438]

Wu X, Morishita W, Beier KT, Heifets BD, and Malenka RC (2021). 5-HT modulation of a medial septal circuit tunes social memory stability. Nature 599, 96–101. 10.1038/s41586-021-03956-8. [PubMed: 34616037]

Yu W, Pati D, Pina MM, Schmidt KT, Boyt KM, Hunker AC, Zweifel LS, McElligott ZA, and Kash TL (2021). Periaqueductal gray/dorsal raphe dopamine neurons contribute to sex differences in pain-related behaviors. Neuron 109, 1365–1380 e1365. 10.1016/j.neuron.2021.03.001. [PubMed: 33740416]

Zachariou V, Bolanos CA, Selley DE, Theobald D, Cassidy MP, Kelz MB, Shaw-Lutchman T, Berton O, Sim-Selley LJ, Dileone RJ, et al. (2006). An essential role for DeltaFosB in the nucleus accumbens in morphine action. Nat Neurosci 9, 205–211. 10.1038/nn1636. [PubMed: 16415864]

Zan GY, Wang YJ, Li XP, Fang JF, Yao SY, Du JY, Wang Q, Sun X, Liu R, Shao XM, et al. (2021). Amygdalar kappa-opioid receptor-dependent upregulating glutamate transporter 1 mediates depressive-like behaviors of opioid abstinence. Cell Rep 37, 109913. 10.1016/j.celrep.2021.109913. [PubMed: 34731618]

Zhang X, Beaulieu JM, Sotnikova TD, Gainetdinov RR, and Caron MG (2004). Tryptophan hydroxylase-2 controls brain serotonin synthesis. Science 305, 217. DOI: 10.1126/science.1097540. [PubMed: 15247473]

Zhu Y, Wienecke CF, Nachtrab G, and Chen X (2016). A thalamic input to the nucleus accumbens mediates opiate dependence. Nature 530, 219–222. 10.1038/nature16954. [PubMed: 26840481]

INCLUSION AND DIVERSITY

We worked to ensure sex balance in the selection of non-human subjects. One or more of the authors of this paper self-identifies as an underrepresented ethnic minority in their field of research or within their geographical location. One or more of the authors of this paper self-identifies as a member of the LGBTQIA+ community. One or more of the authors of this paper received support from a program designed to increase minority representation in their field of research. While citing references scientifically relevant for this work, we also actively worked to promote gender balance in our reference list.

Highlights

- Protracted opioid withdrawal leads to robust social interaction deficits in mice.
- Kappa opioid receptor activation in the NAc is necessary for withdrawal social deficits
- Dynorphin-producing neurons in the DR promote withdrawal social deficits
- KORs reduce 5-HT release in the NAc during withdrawal to mediate social deficits

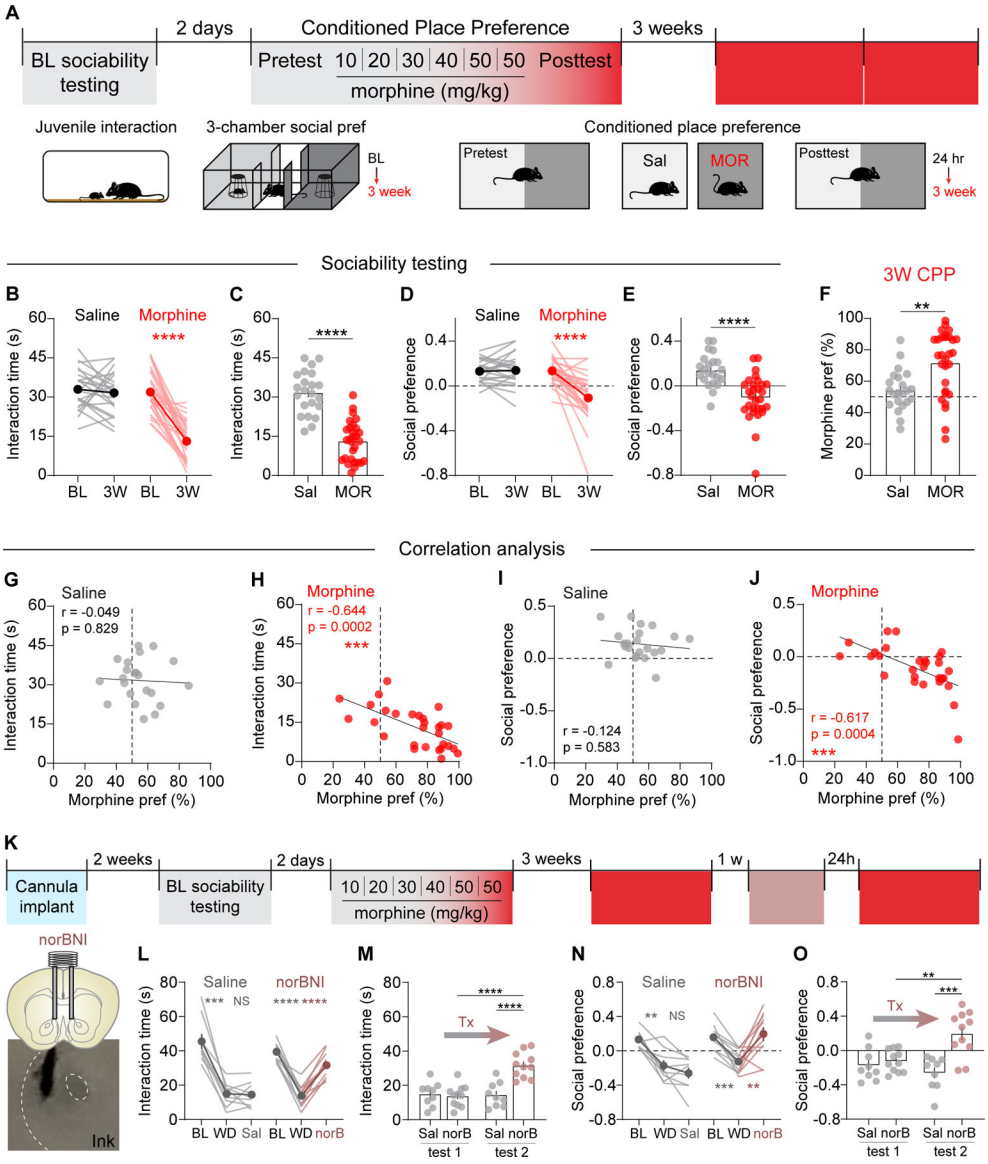

Figure 1. Social deficits during protracted MOR withdrawal require NAc KORs.

(A) Top, timeline of behavioral procedures. Bottom, schematics of juvenile interaction test, 3-chamber social preference assay, and MOR CPP.

(B) Social interaction at baseline (BL) and 3 weeks after saline or morphine injections (3W).

(C) Social interaction at the 3 week time point.

(D) Social preference in the 3-chamber assay.

(E) Social preferences at the 3 week time point.

(F) Long-lasting preference for the MOR-paired chamber.

(G) Saline-treated mice show no correlation between social interaction and chamber preference.

(H) Social interaction during protracted MOR withdrawal is inversely correlated with preference for the MOR-paired chamber.

(I) No correlation between social preference and chamber preference in saline mice.

(J) Social preference during withdrawal is negatively correlated with MOR chamber preference.
(K) Top, experimental procedures. Bottom left, norBNI injection into NAc, scale bar = 100 μm.
(L) All mice show decreased social interaction during withdrawal. Subsequent norBNI treatment increases interaction to baseline levels.
(M) norBNI effects on withdrawal social interaction deficits.
(N) Effects of norBNI in the social preference test.
(O) norBNI effects on reduction in social preference during withdrawal.
**p < 0.01; ***p < 0.001; ****p < 0.0001. Data are represented as mean ± SEM.

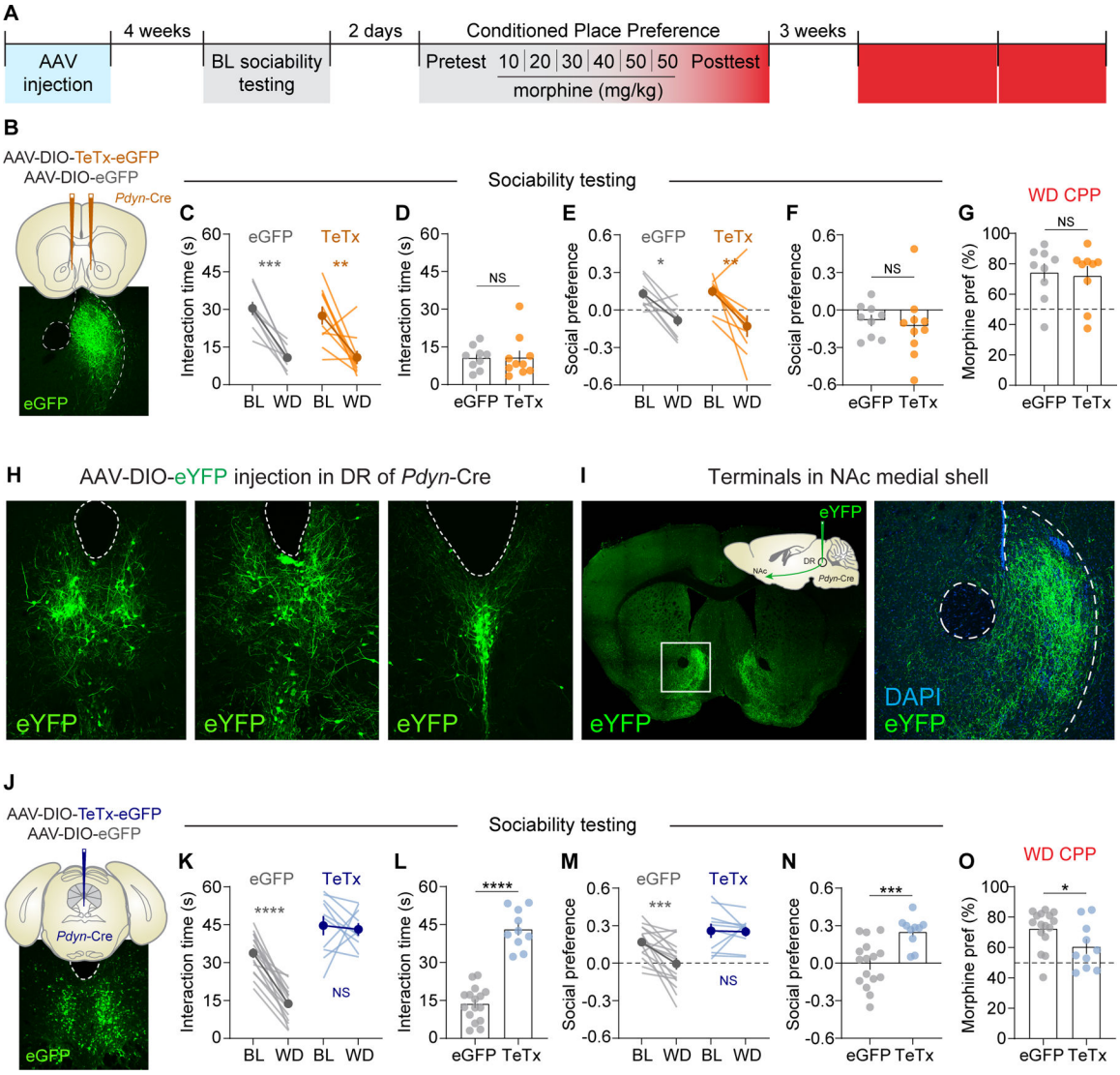

Figure 2. Transmitter release from DR^{Pdyn} neurons is required for sociability deficits during MOR withdrawal.

(A) Experimental procedure.

(B) Viral injection of Cre-dependent TeTx into NAc of *Pdyn*-Cre mice, scale = 100 μm.

(C) Social interaction deficits in mice expressing eGFP and TeTx.

(D) Social interaction during withdrawal.

(E) Similar reductions in social preference in eGFP and TeTx mice.

(F) Social preferences during withdrawal.

(G) MOR CPP during withdrawal.

(H) Injection of AAV-DIO-eYFP into the DR of *Pdyn*-Cre mice revealed dynorphin neurons spanning from anterior (AP −4.2) to posterior (AP −5.0), scale = 100 μm.

(I) Left, projections to NAc medial shell, scale = 500 μm. Right, high magnification image, scale = 100 μm.

(J) Viral injection of Cre-dependent TeTx into DR of *Pdyn*-Cre mice, scale = 100 μm.

(K) Mice expressing TeTx fail to show the characteristic reduction in social interaction.

(L) Social interaction during withdrawal.
(M) TeTx mice maintain social preference.
(N) Social preferences during withdrawal.
(O) MOR CPP during withdrawal is reduced by TeTx.
*p < 0.05; **p < 0.01; ***p < 0.001; ****p < 0.0001. Data are represented as mean ± SEM.

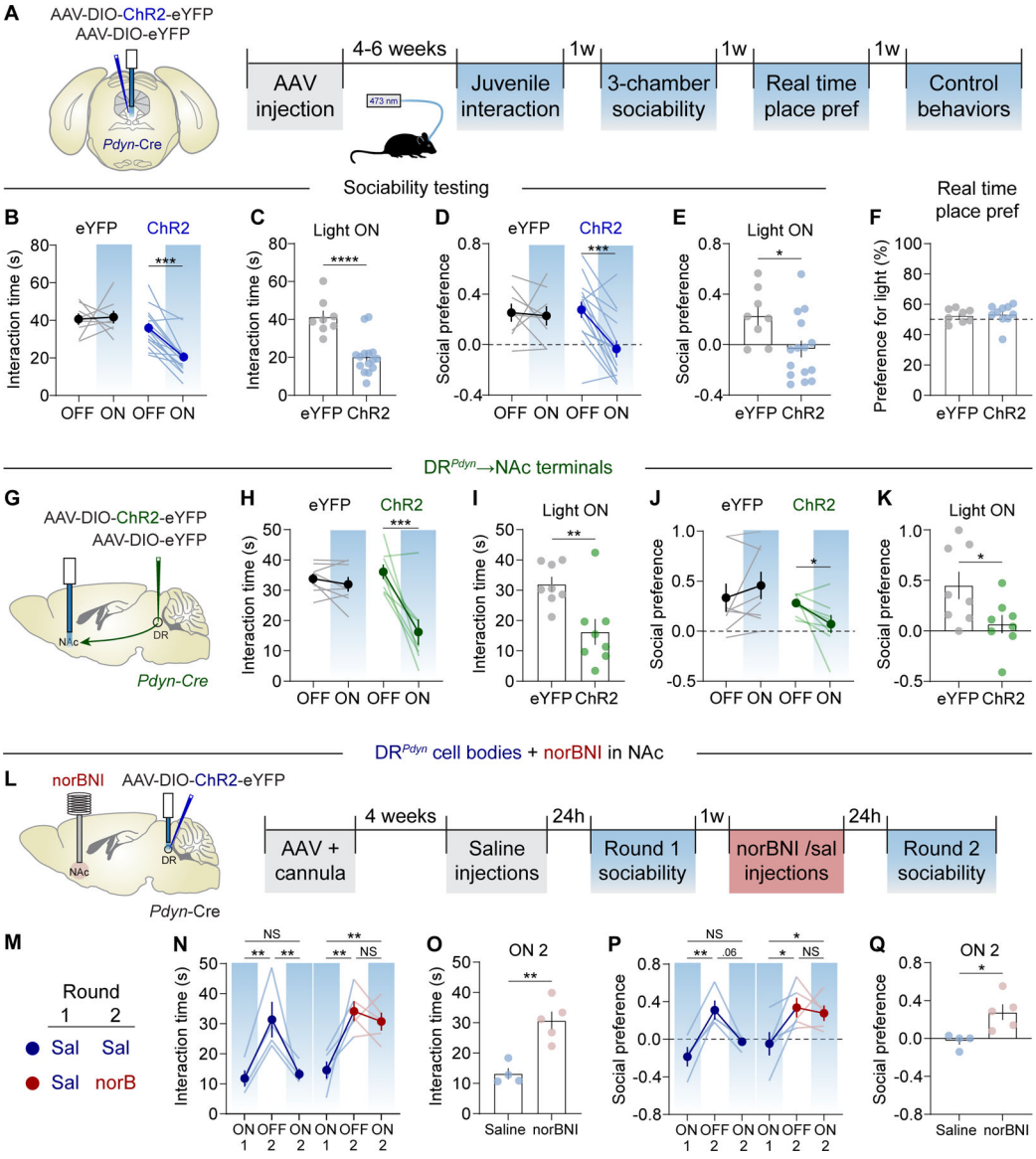

Figure 3. DR^{Pdyn} neurons regulate sociability through KOR activation in NAc.

(A) Left, viral injection and fiber implant. Right, experimental timeline.

(B) Social interaction is reduced by optogenetic stimulation of DR^{Pdyn} neuron cell bodies.

(C) Social interaction when light was on.

(D) Stimulation of DR^{Pdyn} neuron cell bodies also reduced social preference.

(E) Social preference when light was on.

(F) No valence in the real time place preference test.

(G) Viral injection and fiber implant for terminal stimulation.

(H) Activation of DR^{Pdyn} inputs to the NAc medial shell decreased interaction times.

(I) Social interaction when light was on.

(J) Activation of DR^{Pdyn} inputs to the NAc medial shell decreased social preference.

(K) Social preference when light was on.

(L) Left, experimental setup. Right, experimental timeline.

(M) Legend for color-coding of data presentation.
(N) Social interaction times during round 1 with light on and round 2 with light on or off.
(O) Social interaction when light was on during test 2.
(P) Similar results in the 3-chamber assay.
(Q) Social preference when light was on during test 2.
*p < 0.05; **p < 0.01; ***p < 0.001; ****p < 0.0001. Data are represented as mean ± SEM.

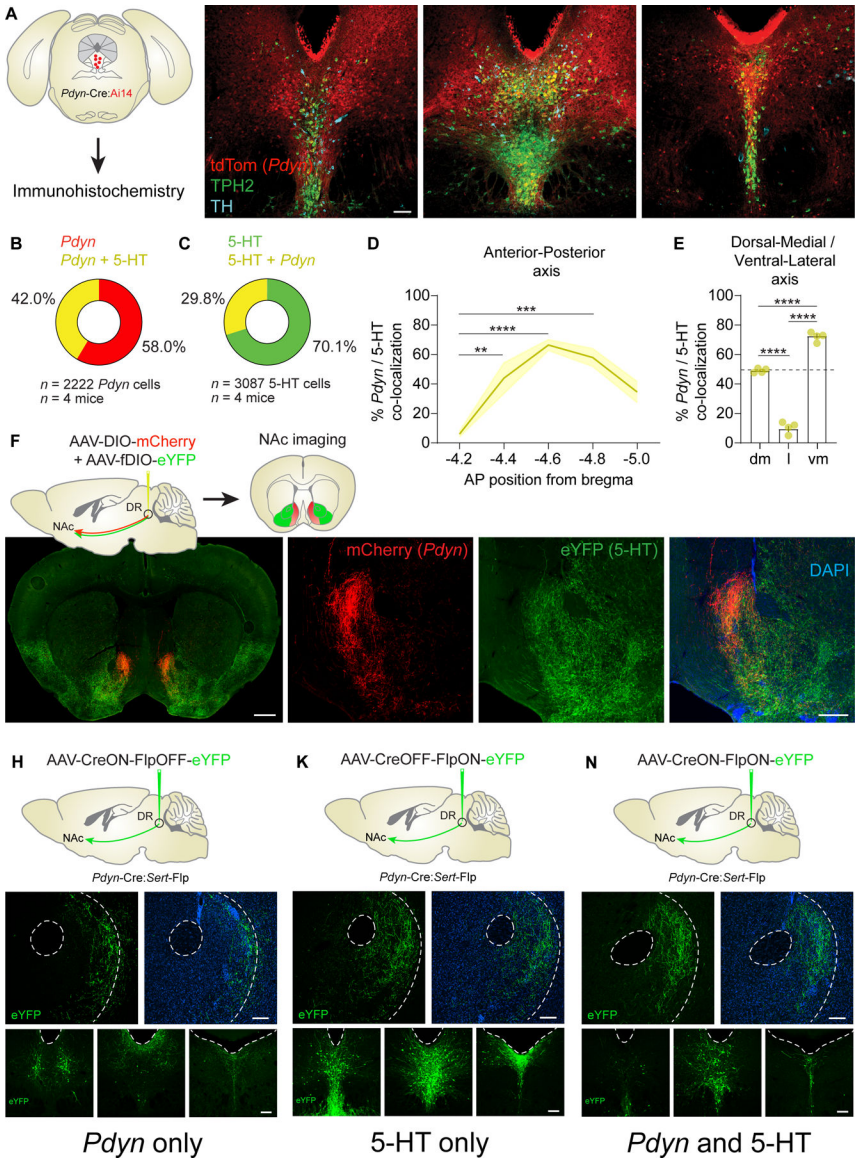

Figure 4. DR^{Pdyn} neurons overlap with DR$^{5\text{-}HT}$ neurons and project to the NAc medial shell.

(A) Left, *Pdyn*-Cre:Ai14 reporter mouse analysis. Right, *Pdyn* cell co-localization with TPH2 and TH, scale = 100 μm.

(B) Proportion of DR^{Pdyn} neurons that are also 5-HTergic.

(C) Proportion of 5-HT neurons that also express *Pdyn*.

(D) Distribution of *Pdyn*/5-HT neurons across the DR AP axis.

(E) Distribution of *Pdyn*/5-HT neurons across the DM and VL axes.

(F) Viral injection into *Pdyn*-Cre:*Sert*-Flp mice.

(G) Left, wide field image of NAc from *Pdyn*-Cre:*Sert*-Flp mouse injected with cocktailed fDIO-eYFP and DIO-mCherry, scale = 500 μm. Right, high magnification *Pdyn* and 5-HT axons targeting the NAc, scale = 100 μm.

(H) Viral injection of CreON-FlpOFF-eYFP to infect *Pdyn* neurons that lack 5-HT.

(I) 5-HT negative DR^{Pdyn} axons in the NAc, scale = 100 μm.

(J) Distribution of 5-HT negative DR^{Pdyn} neurons across the DR, scale = 100 μm.
(K) Viral injection of CreOFF-FlpON-eYFP to infect 5-HT neurons that lack *Pdyn*.
(L) *Pdyn* negative DR$^{5\text{-}HT}$ axons in the NAc, scale = 100 μm.
(M) Distribution of *Pdyn* negative DR$^{5\text{-}HT}$ neurons across the DR, scale = 100 μm.
(N) Viral injection of CreON-FlpON-eYFP to infect *Pdyn* neurons that contain 5-HT.
(O) 5-HT positive DR^{Pdyn} axons in the NAc, scale = 100 μm.
(P) Distribution of 5-HT positive DR^{Pdyn} neurons across the DR, scale = 100 μm.
**p < 0.01; ***p < 0.001; ****p < 0.0001. Data are represented as mean ± SEM.

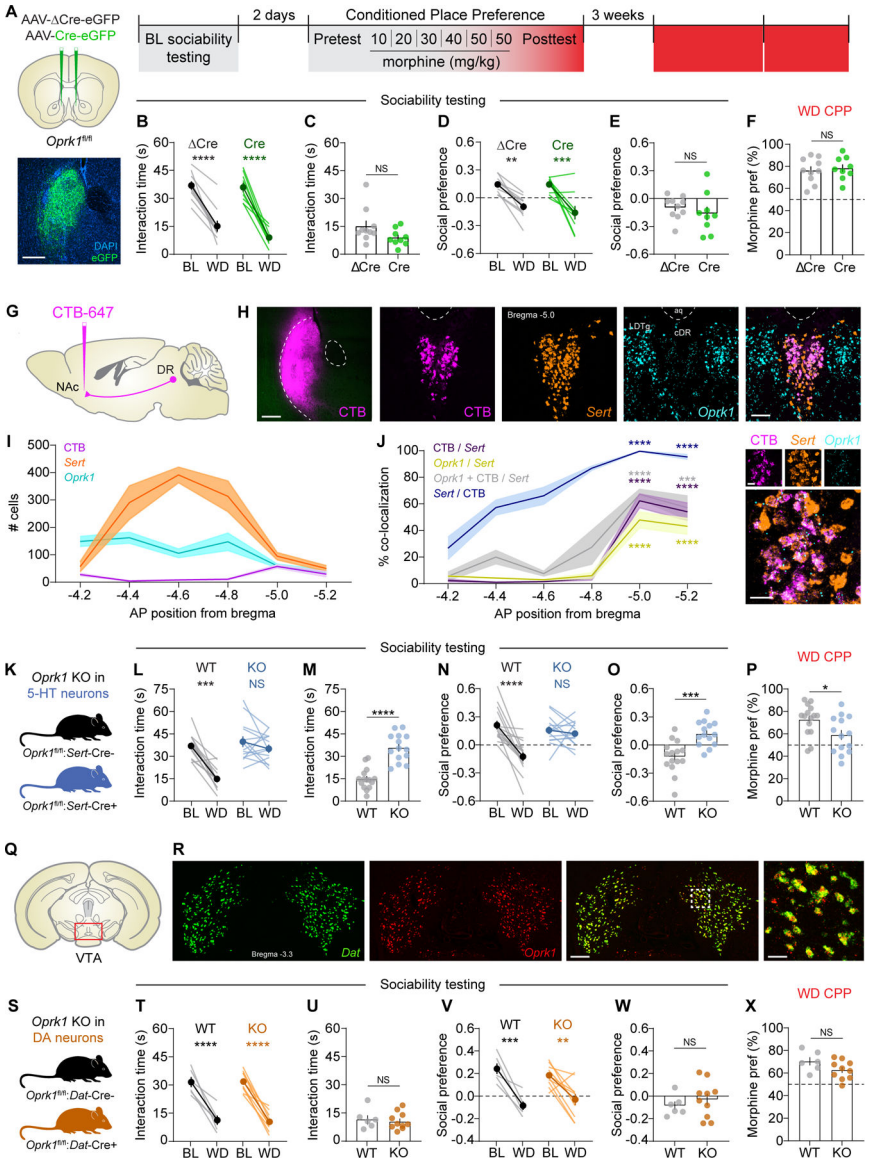

Figure 5. KORs in 5-HT neurons are critical for sociability deficits during opioid withdrawal.

(A) Left, schematic and image of viral injection in NAc, scale = 100 μm. Right, experimental timeline.

(B) Deletion of KORs in NAc neurons did not affect social interaction during protracted opioid withdrawal.

(C) Social interaction deficits during withdrawal.

(D) Minimal effect on social preference during protracted withdrawal.

(E) Social preference deficits during withdrawal.

(F) No effect on MOR CPP during withdrawal.

(G) CTB-647 injection into NAc for retrograde tracing in the DR.

(H) Left, CTB injection in the NAc medial shell, scale = 100 μm. Right, retrolabeled cells in the caudal DR positive for *Sert* and *Oprk1* mRNA, scale = 50 μm. Bottom right, magnified image, scale = 10 μm.

(I) Counts of cells positive for CTB, *Sert*, and *Oprk1* across the AP axis of the DR.
(J) Co-localization between CTB, *Sert*, and *Oprk1* across the AP axis.
(K) Genetic deletion of KORs in 5-HT neurons.
(L) Deletion of KORs from *Sert* neurons prevented social interaction deficits.
(M) Social interaction deficits during withdrawal.
(N) Deletion of KORs from *Sert* neurons prevented social preference deficits.
(O) Social preference deficits during withdrawal.
(P) Reduced MOR CPP during withdrawal.
(Q) Coronal section containing the VTA.
(R) Left, overlap between *Dat* and *Oprk1* mRNA in the VTA, scale = 100 μm. Far right, high magnification image, scale = 20 μm.
(S) Genetic deletion of KORs in DA neurons.
(T) Deletion of KORs from *Dat* neurons had no effect on social interaction deficits.
(U) Social interaction deficits during withdrawal.
(V) Deletion of KORs from *Dat* neurons also had no effect on social preference deficits.
(W) Social preference deficits during withdrawal.
(X) Similar MOR CPP during withdrawal.
*$p < 0.05$; **$p < 0.01$; ***$p < 0.001$; ****$p < 0.0001$. Data are represented as mean ± SEM.

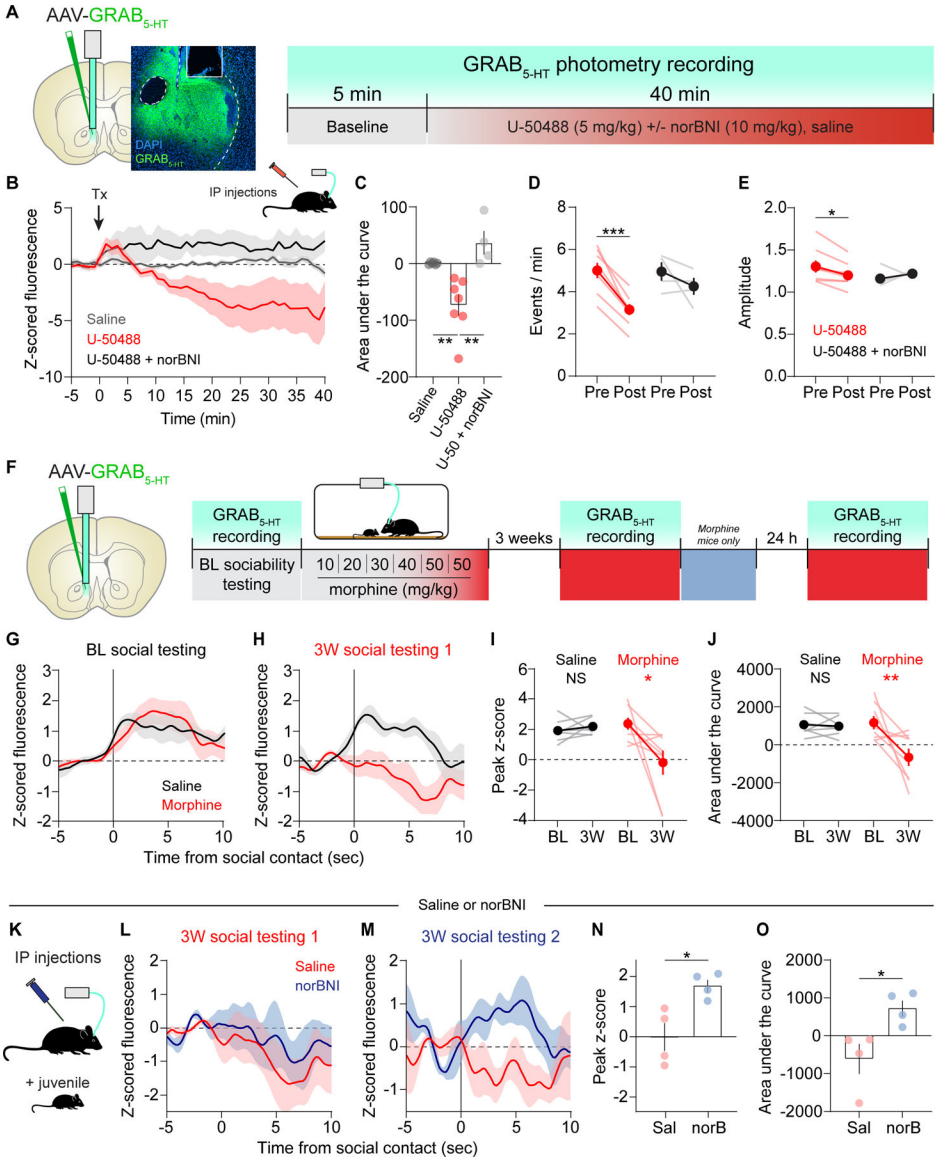

Figure 6. KORs inhibit NAc 5-HT release during protracted opioid withdrawal.

(A) Left, schematic of fiber photometry setup and image of $GRAB_{5\text{-}HT}$ in the NAc, scale = 100 μm. Right, timeline of recordings during drug administration.

(B) Average $GRAB_{5\text{-}HT}$ fluorescence after injection of saline, U-50488 (5 mg/kg), or U-50488 pretreated with norBNI (10 mg/kg).

(C) Area under the curve after drug injections.

(D) Transient event frequency pre- and post-injection.

(E) Transient event amplitude pre- and post-injection.

(F) Left, $GRAB_{5\text{-}HT}$ recording site. Right, experimental timeline.

(G) Average $GRAB_{5\text{-}HT}$ fluorescence during the first direct social contact in the baseline social interaction test.

(H) Average $GRAB_{5\text{-}HT}$ fluorescence at the 3 week time point.

(I) Peak z-score during social contact.

(J) Area under the curve during social contact.
(K) Experimental setup. Mice received an injection of saline or norBNI (10 mg/kg) 24 hrs prior to a second social test and recording during withdrawal.
(L) Average $GRAB_{5\text{-}HT}$ fluorescence during the first direct social contact in MOR-treated mice, split into saline and norBNI groups. This panel represents the same data as the Morphine curve in panel H.
(M) Average $GRAB_{5\text{-}HT}$ fluorescence in social test 2 after norBNI administration.
(N) Peak z-score during social contact.
(O) Area under the curve during social contact.
*$p < 0.05$; **$p < 0.01$; ***$p < 0.001$. Data are represented as mean ± SEM.

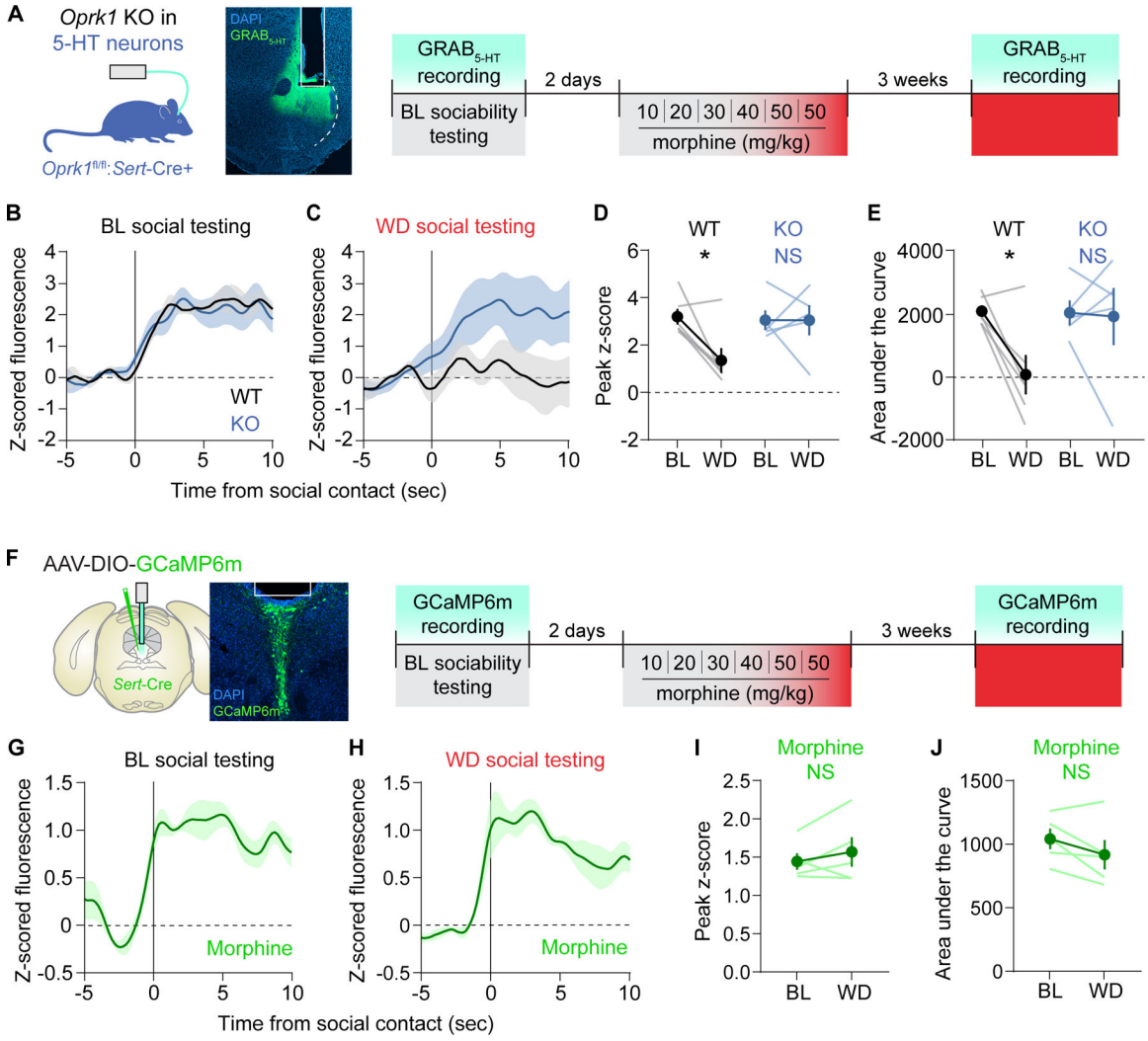

Figure 7. KORs on 5-HT inputs regulate 5-HT release in NAc during opioid withdrawal.

(A) Left, experimental design and image of $GRAB_{5\text{-}HT}$ in the NAc, scale = 200 μm. Right, experimental timeline.

(B) Average $GRAB_{5\text{-}HT}$ fluorescence time-locked to the first direct social contact during the baseline social interaction test.

(C) Average $GRAB_{5\text{-}HT}$ fluorescence during withdrawal.

(D) Peak z-score during social contact.

(E) Area under the curve during social contact.

(F) Left, schematic and image of DIO-GCaMP6m and fiber placement in the cDR of *Sert*-Cre mice, scale = 100 μm. Right, experimental timeline.

(G) Average GCaMP6m fluorescence during social contact in the baseline social interaction test.

(H) Average GCaMP6m fluorescence during withdrawal.

(I) Peak z-score during social contact.

(J) Area under the curve during social contact.

*p < 0.05. Data are represented as mean ± SEM.

Table 1.

Key resources table

REAGENT or RESOURCE	SOURCE	IDENTIFIER
Antibodies		
TPH2, rabbit	Novus Biologicals	NB100–74555
TH, mouse	Millipore	RRID: AB_2201528
mCherry, rat	Millipore	MAB131873
GFP, chicken	Aves Labs	RRID: AB_10000240
Bacterial and virus strains		
AAVdj-hSyn-Cre-eGFP	Stanford Gene Vector and Virus Core	GVVC-AAV-117
AAVdj-hSyn-ΔCre-eGFP	Stanford Gene Vector and Virus Core	GVVC-AAV-118
AAVdj-CMV-DIO-eGFP-2A-TeTx	Stanford Gene Vector and Virus Core	GVVC-AAV-71
AAVdj-CMV-eGFP-2A-TeTx	Stanford Gene Vector and Virus Core	GVVC-AAV-70
AAVdj-CMV-DIO-eGFP	Stanford Gene Vector and Virus Core	GVVC-AAV-12
AAVdj-EF1a-DIO-hChR2(H134R)-eYFP	Stanford Gene Vector and Virus Core	GVVC-AAV-38
AAVdj-EF1a-DIO-eYFP	Stanford Gene Vector and Virus Core	GVVC-AAV-13
AAVdj-EF1a-DIO-mCherry	Stanford Gene Vector and Virus Core	GVVC-AAV-14
AAVdj-EF1a-fDIO-eYFP	Stanford Gene Vector and Virus Core	GVVC-AAV-86
AAVdj-hSyn-CreON-FlpOFF-eYFP-WPRE	Stanford Gene Vector and Virus Core	GVVC-AAV-80
AAVdj-hSyn-CreOFF-FlpON-eYFP-WPRE	Stanford Gene Vector and Virus Core	GVVC-AAV-82
AAVdj-hSyn-CreON-FlpON-eYFP-WPRE	Stanford Gene Vector and Virus Core	GVVC-AAV-78
AAVdj-hSyn-FLEX-mGFP-2A-synaptophysin-mRuby	Stanford Gene Vector and Virus Core	GVVC-AAV-100
AAVdj-EF1a-DIO-GCaMP6m	Stanford Gene Vector and Virus Core	GVVC-AAV-92
AAV9-hSyn-GRAB5HT 2h (5-HT 3.5)	WZ Biosciences	Lot# 20210901
AAV9-hSyn-GRABDA 2m (DA 4.4)	WZ Biosciences	Lot# 20210920
Biological samples		
Chemicals, peptides, and recombinant proteins		
Morphine sulfate	Sigma Aldrich	M8777
Norbinaltorphimine dihydrochloride (norBNI)	Tocris	0347 (discontinued)
(±)-U-50488 hydrochloride	Tocris	0495
MDMA	NIDA	Cat# 7405–001
Cholera Toxin subunit B, Alexa Fluor 647 conjugate	Invitrogen	C34778
Aticaprant (JNJ-67953964, CERC-501, LY2456302)	Med Chem Express	HY-101718
NBQX	Tocris	0373
D-AP5	Tocris	0106

REAGENT or RESOURCE	SOURCE	IDENTIFIER
CGP55845	Tocris	1248
Critical commercial assays		
Deposited data		
Experimental models: Cell lines		
Experimental models: Organisms/strains		
Wild-type C57BL/6J	Jackson Laboratory	RRID: IMSR_JAX:000664
B6;129S-*Pdyn*$^{tm1.1(cre)Mjkr}$/LowlJ (*Pdyn*-Cre)	Jackson Laboratory	RRID: IMSR_JAX:027958
Tg(*Slc6a4*-Cre)ET33Gsat (*Sert*-Cre)	Jackson Laboratory	MGI:3836639
B6.SJL-*Slc6a3*$^{tm1.1(cre)Bkmn}$/J (*Dat*-Cre)	Jackson Laboratory	RRID: IMSR_JAX:006660
B6.Cg-*Slc6a4*$^{tm1.1(flpo)Luo}$/J (*Sert*-Flp)	Gift from L. Luo; Jackson Laboratory	RRID: IMSR_JAX:034050
B6;129S-*Oprk1*$^{tm2.1Kff}$/J (*Oprk1*$^{fl/fl}$)	Jackson Laboratory	RRID: IMSR_JAX:030076
B6.Cg-*Gt(ROSA)26Sor*$^{tm14(CAG-tdTomato)Hze}$/J (Ai14)	Jackson Laboratory	RRID: IMSR_JAX:007914
Oligonucleotides		
RNAscope probe: *Slc6a4*-C1 (*Sert*)	Advanced Cell Diagnostics	315851
RNAscope probe: *Slc6a3*-C1 (*Dat*)	Advanced Cell Diagnostics	315441
RNAscope probe: *Oprk1*-C3	Advanced Cell Diagnostics	316111
Recombinant DNA		
Software and algorithms		

REAGENT or RESOURCE	SOURCE	IDENTIFIER
BIOBSERVE behavioral research VIEWER	BIOBSERVE	http://www.biobserve.com/behavioralresearch/
FIJI	Schindelin et al., 2012	RRID:SCR_002285
NIS-Elements AR 5.02	Nikon	
MATLAB R2021a	MathWorks	https://www.mathworks.com/products/matlab.html
Syanptosoft	Molecular Devices	
Excel	Microsoft	RRID:SCR_016137
Illustrator CS6	Adobe	https://www.adobe.com/products/illustrator.html
Prism 9	GraphPad	https://www.graphpad.com/scientific-software/prism/
Other		